Marine and Petroleum Geology 170 (2024) 107125

Contents lists available at ScienceDirect

Marine and Petroleum Geology

journal homepage: www.elsevier.com/locate/marpetgeo

Paleogeographic reconstruction and sedimentary evolution of tidal-dominated estuarine depositional systems: Insights from the campanian M1 sandstone formation, Oriente Basin, Ecuador

Sicheng Zhu [a], Panke Sun [a,*], Kexin Zhang [b], Chaoqian Zhang [b], Qi Zhang [c], Bin Li [a], Jiang Wang [a], Shiyi Jiang [a], Liyin Bao [a], Guangbin Jing [a], Zhangxing Chen [d], Huaimin Xu [a]

[a] College of Geosciences, China University of Petroleum-Beijing, Beijing 102249, China
[b] Research Institute of Petroleum Exploration and Development, PetroChina, Beijing 100083, China
[c] Geological Research Institute of Fourth Oil Production Plant, Daqing Oilfield Co., Ltd, Daqing 163511, China
[d] Eastern Institute of Technology, Ningbo, 315200, China

ARTICLE INFO

Keywords:
Oriente Basin
M1 Sandstone Formation
Tidal-dominated estuary
Estuarine facies model
Coastal system evolution

ABSTRACT

The Oriente Basin is a back-arc basin located east of the Ecuadorian Andes in South America. Evidence suggests that during the Cretaceous period, the basin's margins received a terrigenous shallow marine sedimentation. Due to regional variations in accommodation and depositional controlling factors near a shoreline, the sedimentary environments in the fluvial-marine transitional zones exhibit considerable variability. In this study, we analyzed the sedimentological characteristics of the M1 Sandstone Formation unit (~83 Ma-72 Ma), which comprises a set of ancient estuarine deposits preserved in the northern part of the basin. We quantified the impact of mixed hydrodynamic processes on the distribution of tidal-dominated estuarine facies and discussed the development conditions and evolutionary processes of an estuarine formation under the background of persistent transgression. Core, well log, and seismic data provide evidence for reconstructing the tidal-dominated estuarine environment. In the core section, we identified 14 lithofacies and 7 major facies association types. The frequent occurrence of sedimentary structures associated with tidal currents indicates that tidal processes extensively reworked the deposits. The spatial distribution trends of facies associations reveal the evolution of mixed hydrodynamic conditions dominated by tidal processes in the estuary and allow us to divide the M1 Sandstone Formation into four depositional periods: the initial development, rapid development, decline, and the post-infilling open coast tidal flat development periods. Furthermore, through a systematic analysis of hydrodynamic conditions and sediment distributions, we identified multiple depositional centers in the tidal-dominated estuary influenced by different hydrodynamic processes. These correspond to the upstream fluvial-dominated tidal point bar depositional region, the middle mixed-energy depositional interaction zone, and the downstream tidal-dominated tidal sand bar depositional region. In these regions, the substantial accumulation of sandy deposits, represented by tidal sand bars, reflects the high accommodation space characteristic of tidal-dominated estuaries. Our findings indicate that the slow subsidence of a broad and gently sloping coastal topography, stable material transport, and sea level change dominated by marine transgression ensured the necessary accommodation for the development of the estuary in the M1 Sandstone Formation. The sedimentological study of the M1 Sandstone Formation provides a case for understanding the sedimentary evolution in fluvial-marine transitional zones.

1. Introduction

Tidal-dominated estuaries are highly dynamic depositional settings exhibiting erosional geomorphological features, widely developed in coastal regions significantly influenced by tides. When river and marine waters converge at an estuary, the cumulative effects of fluvial, tidal, and wave currents create gradients of environmental characteristics, such as water salinity and turbidity, along the perpendicular direction of

* Corresponding author.
E-mail address: sunpk@cup.edu.cn (P. Sun).

https://doi.org/10.1016/j.marpetgeo.2024.107125
Received 4 August 2024; Received in revised form 16 September 2024; Accepted 18 September 2024
Available online 28 September 2024

a shoreline (Boyd et al., 2006; Dalrymple et al., 2011; Jay et al., 2015). This sedimentary process, driven by various hydrodynamic conditions, is known as a mixed hydrodynamic process and directly affects the distribution of materials in clastic coastal zones (Wells et al., 2007; Yoshida et al., 2007; Fenies et al., 2010; Ainsworth et al., 2011; Dashtgard and La Croix, 2015). In the classification of clastic coastal systems, tidal-dominated estuaries represent a tidal-dominated end-member environment, where tidal processes play a more critical role in the transport and reworking of sediments (Boyd et al., 1992; Collins et al., 2021; Wehrmann, 2014). Sedimentological and tidal dynamics studies indicate that tidal energy is enhanced when passing through a region of estuarine mouth due to constrictive geomorphology, as a result of tidal resonance and increased tidal prisms (Sztanó and De Boer, 1995; Dalrymple et al., 2011; Burchard et al., 2018). This phenomenon of tidal enhancement is more pronounced during a marine transgressive stage (Tessier et al., 2012a). As tidal currents propagate further upstream, tidal energy gradually dissipates due to factors such as bed friction and fluvial action, eventually diminishing near the tidal limit (Wang et al., 2002). Notably, the intensity of tidal influence varies across different depositional regions within a tide-dominated estuary, reflected in the variations in grain size, sedimentary structures, and facies associations (Dalrymple and Choi, 2007; Coughenour et al., 2009a; Dashtgard et al., 2012). Moreover, as a bidirectional flow, the hydrodynamic intensity and flow direction of tidal currents change periodically with flood and ebb tide processes, unlike river and wave currents (Longhitano et al., 2012). This periodicity of tidal currents can be preserved in specific sedimentary structures, where it is fully recorded, such as tidal rhythmites with alternating sand-mud layers and bidirectional cross-bedding reflecting alternating flow directions (Visser, 1980; Smith, 1988; Tessier and Gigot, 1989; Stupples and Plater, 2007; Longhitano, 2011). Additionally, these rock records offer valuable insights into identifying tidal processes, understanding the formation of ancient estuarine deposits, and reconstructing estuarine environmental evolution (Aldinucci et al., 2007; Tessier et al., 2010; Dalrymple et al., 2015; Gingras and Zonneveld, 2015; Jablonski and Dalrymple, 2016; Souza et al., 2023).

Furthermore, a sequence stratigraphic theory indicates that in high-energy coastal zones with marine transgression context and relatively weak sediment supply, estuarine systems with undercompensated geomorphology are likely to form (Allen et al., 1980; Gregoire et al., 2017; Phillips et al., 2020a,b; Peng et al., 2022). The evolution of estuarine systems is inherited from incised valley systems formed by previous fluvial erosion of a substrate or from eroded areas of delta plains (Plint and Wadsworth, 2003; Dalrymple and Choi, 2007; Zhang et al., 2014a; Wang et al., 2019). Estuaries typically develop during transgressive stages, where continuous rise in the relative sea level keeps the estuary in an undercompensated state, allowing sand and mud deposits from rivers and the sea to be fully captured and preserved (Yoshida et al., 2001; Feldman et al., 2008; Tessier B. et al., 2010; Li et al., 2018). As a result, estuaries, despite their relatively short lifecycles compared to other environments, form sizeable and well-preserved sandy reservoirs. The input of sediment from both land and sea, along with a rate of sea-level fluctuations, fundamentally determines the overall sedimentary scale of an estuary (Van Den Berg et al., 2007). However, at various stages of estuarine evolution, differences in local hydrodynamic energy distribution directly impact the spatial distribution patterns of sand and mud components (Dalrymple et al., 1991; Hayes and FitzGerald, 2013; Todd et al., 2014). Tessier (2012) compared a series of modern sedimentary cases of tidal-dominated estuaries, highlighting significant diversity in the geometric shapes and relative proportions of facies in their sedimentary fill characteristics. Therefore, when studying the sedimentation and evolution of estuarine environments, it is essential to gather extensive evidence, including hydrodynamic conditions, relative sea-level changes, and sediment supply (Chaumillon et al., 2010; Tessier et al., 2012a). Especially in the study of ancient estuarine deposits, the limited rock records and the lack of hydrodynamic data, such as water depth and flow velocity, lead to multiple interpretations of the environment.

While studies on modern estuaries offer more direct sedimentological evidence, preserved estuarine deposits in ancient strata are equally valuable. The Oriente Basin is one of the major hydrocarbon-bearing basins in South America (White et al., 1995; Jaillard et al., 1997; Baby et al., 2004). During the Cretaceous period, this basin underwent several large-scale marine transgressions (Vallejo et al., 2021). Among these, the M1 Sandstone Formation is a well-preserved clastic deposit from the Campanian period of the Late Cretaceous, with sand bodies concentrated in the eastern part of the basin (Jaillard et al., 2005; Vallejo et al., 2017). The clastic components reflect significant paleogeographic changes and coastal fluctuations over a span of up to 200 km near an ancient shoreline (Vallejo et al., 2021). Due to regional variations in accommodation and depositional controlling factors near the shoreline, the M1 Sandstone Formation has the potential for developing estuarine systems (Barragán et al., 2004).

In this study, we examine a set of ancient clastic deposits preserved in the M1 Sandstone segment in the northern part of the Oriente basin. These deposits show strong tidal influence and contain sedimentary indicators of an estuarine environment. The objectives of this study include: (i) identifying the lithofacies types of the tidal-dominated estuary and clarifying the characteristics of facies associations using core and well log data; (ii) exploring the mixed hydrodynamic processes in the tidal-dominated estuary and their relationship with sediment distributions; (iii) proposing a facies model of the tidal-dominated estuary under mixed hydrodynamic processes; and (iv) reconstructing a paleogeographic development model for the M1 Sandstone Formation and discussing the impacts of tectonic activities, sea-level changes, and sediment supply on the evolution of the estuarine environment within the context of a broad and gentle shoreline.

2. Geological setting

2.1. Tectonic and sedimentary characteristics

The Oriente Basin is situated in the northwestern part of South America, between the Andes orogen and the Guiana Shield (Fig. 1A), forming part of the Andean back-arc basin system (Gombojav and Winkler, 2008; Baby et al., 2013). Drilling records reveal that this basin has accumulated approximately 5000 m of Mesozoic to Cenozoic sediment layers (Baby et al., 2004). Its formation traces back to the late Triassic rift expansion era, around 202 million years ago, evidenced by early marine sediment accumulation (Spikings et al., 2015). During Middle Jurassic to Middle Late Jurassic (~180 Ma-157 Ma), the basin began to experience tectonic instability and an extensional tectonic regime, influenced by localized southeastward subduction. This phase began with the development of the calc-alkaline magmatic arc in the Colombian segment, whose formation mechanism corresponds to the influence of Tethyan subduction as proposed in the 'Tethys-controlled evolution' model (Jaillard et al., 1990). As extension continued and a basement paleo-high formed, Oriente basin developed into two back-arc sub-basins, corresponding to the gradual subsidence deposits of the Sacha-Shushufindi Corridor and the semi-grabens of the Capiron-Tiputini system, which established the basin's initial tectonic arrangement (Horton, 2018; Zamora and Gil, 2018; Spikings and Simpson, 2014; Spikings et al., 2019). During Middle Late Jurassic to Early Cretaceous (~157 Ma-140 Ma), the basin space underwent modifications heavily driven by the Pacific northeastward subduction. The western margin of the basin recorded igneous intrusions formed by magmatic activity near the Cordillera Mountains. (Pratt et al., 2005). Meanwhile, the continued back-arc extension and marine transgression during this period contributed to the deposition of the Chapiza Group (Romeuf et al., 1995).

In the Early Cretaceous (~140 Ma-125 Ma), the collision of allochthonous terranes along the Northern South American plate margin led to the formation of an unconformity surface and paleotopographic

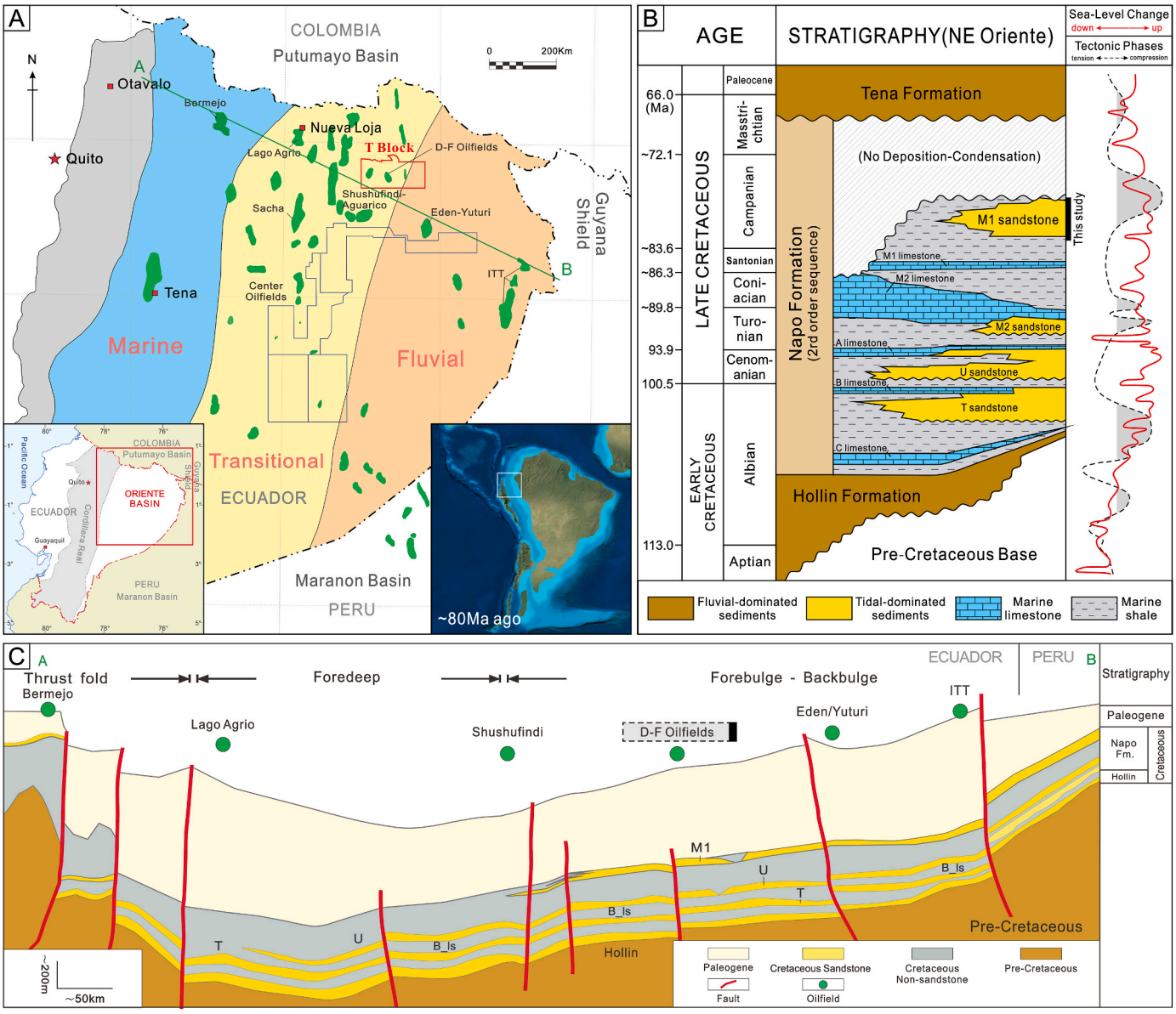

Fig. 1. (A) The location of the Oriente Basin, Ecuador, and paleogeographic map of the Napo Formation, showing the marine-fluvial transitional area, oil fields and blocks, and palaeoceanographic reconstructions for the Late Cretaceous (Campanian, ~80 Ma ago) in South America (modified from White et al., 1995; Estupiñan et al., 2010; Scotese, 2021). (B) Lithostratigraphic chart for Cretaceous strata of the Oriente Basin with sea-level change curve and tectonic phase curve (modified from Jaillard and Soler, 1996). (C) Transverse cross section of the Oriente basin showing the general structure and main sandstone formation (modified from Yang et al., 2017). See Fig. 1A for cross-section location.

depressions at the base of the Cretaceous strata. After that, the Oriente Basin transitioned into a mild subsidence phase during the late Early Cretaceous to Late Cretaceous (~125 Ma-72 Ma). Eastward from the basin's center, sedimentary layers progressively taper, interfacing with the Gondwana shield (Baby et al., 2004). The basin's material inputs were chiefly derived from the erosion of ancient sediments in eastern Gondwana (Ruiz et al., 2007a,b; Martin-Gombojav and Winkler, 2008; Vallejo et al., 2017; Gutiérrez et al., 2019). Due to its proximity to the continental margin's shallow sea, the strata incorporate marine mud and carbonate rock components, along with high-energy, hydrodynamically modified sandy sediments of continental origin (Barragàn et al., 2005). The deposits from this era were relatively stable and continuous, reflecting the expansion of the accommodation, influenced by both the basin's subsidence and sea-level fluctuations. Towards the end of Late Cretaceous (~72 Ma), tectonic events associated with the accretion of oceanic terranes caused the uplift of Ecuadorian active margin, resulting in a series of sedimentary hiatuses, marking the gradual evolution of the Oriente Basin into a foreland evolution (Baby et al., 1999; Barragán and Baby, 2004; Jaillard, 2022).

The Cretaceous rocks in the Oriente Basin comprise a series of multi-phase, staged transgression-regression cycles, deposited from the Albian to the Maastrichtian stages (Fig. 1B) (Jaillard et al., 1997; Baby et al., 2004). During the Albian period, compressional and contractional deformation from the direction of Peru led the basin into a subsidence phase, providing continuously increasing accommodation space for sediment accumulation (Baby et al., 2004; Horton, 2018; Chen et al., 2019; Spikings et al., 2019). The coupling of subsidence rates and sea-level changes ensured a high consistency between facies evolution and water depth within the strata. Additionally, limited sediment supply during this period resulted in relatively well-preserved deposits, which can be divided into the primarily terrestrial fluvial deposits of the Hollin Formation (approximately 120 Ma-100 Ma), the multi-phase marine and

coastal clastic deposits of the Napo Formation (approximately 100 Ma-72 Ma), and the progradational delta deposits of the Tena Base Formation (approximately 72 Ma-66 Ma) (Jaillard et al., 1997; Baby et al., 2004; Gutiérrez et al., 2019). This sequence includes at least six third-order sequences, each containing characteristic sandstone layers, including, from bottom to top, the Hollin Formation, the T Sandstone, U Sandstone, M2 Sandstone, and M1 Sandstone of the Napo Formation, as well as the Basel Tena Sandstone (Jaillard et al., 1997; Baby et al., 2004; Vallejo C. et al., 2021). The target interval of this study is the M1 Sandstone Formation (~83 Ma-72 Ma), which corresponds to the final third-order transgression-regression cycle within the Napo Formation.

Previous studies indicate that sea levels remained relatively high during the Cretaceous period, reaching the peak during the Cenomanian. (McDonough and Cross, 1991; Vellekoop et al., 2017; Aguirre-Urreta et al., 2019). Fluctuations in relative sea level caused each third-order sequence within the Napo Group to develope nearly four distinct types of sedimentary deposits: transgressive sandstone, bioclastic limestone, laminated shale, and laminated limestone (Jaillard et al., 1996; Baby et al., 2004). The prevalence of these rock types indicates that regional sedimentary conditions were predominantly dictated by shifts in relative sea levels (Marzouk and Youssef, 2008; Ye, 2014). Evidence from this era suggests that the basin was covered by a continental margin-sea that connected the northern and southern regions. The basin's eastern margin, with its relatively gentle slope, allowed marine influences to permeate the shoreline-adjacent sediments (Louterbach et al., 2014; Spikings et al., 2019; Vallejo C. et al., 2021). During periods of rapid transgression, the basin experienced a low sedimentation rate, leaving the accommodation only partially filled by marine sediments (Zuniga et al., 2021a). This resulted in the influx of relatively high-energy nearshore sandy deposits and shallow marine bioclastic limestones into the basin, transported by marine water erosion, and forming erosional contacts with older strata. As the sea level continued to rise, thick layers of marine mudstone and limestone successively and stably overlaid the earlier high-energy shallow marine deposits. This alternation pattern signifies a transition from open marine environments to a moderate energy, and restricted low-energy depositional periods with limited water circulation (Jaillard et al., 1996).

2.2. M1 sandstone formation

The study area is located in the eastern slope zone of the Oriente Basin, near the central part of the basin (Fig. 1A). The focal point of this study is the M1 Sandstone segment, a significant stratigraphic unit from the late Cretaceous Campanian stage (~83 Ma-72 Ma), with depths reaching up to 3500 m (Baby et al., 2004). Although the M1 Sandstone segment spans a mere 30 m in thickness, its significance as the primary hydrocarbon reservoir within the Napo Group remains undiminished (Zhongzhen et al., 2021a,b). Owing to the persistent compressive forces exerted by the western thrust faults (~90 Ma-), the M1 sandstone layer is predominantly situated in the basin's eastern region (Fig. 1C), but is also present in the western part (Jaillard et al., 1997).Consequently, the study area is likely aligned with the most distal sand deposition zone of the M1 sandstone segment (Baby et al., 2004; Vallejo et al., 2017).

Based on detailed biostratigraphic and sedimentological studies, the M1 Sandstone Formation is a lens deposits of sandstone formed during a minor marine transgression, and it exhibits erosional contacts with both the underlying Upper Napo Shale and the overlying Lower Tena Formation (Jaillard et al., 1997). In contrast to the sedimentary evidence suggesting river-dominated or tidal-influenced river deposits in lowstand systems tracts, as observed in the lower T and U Sandstone Formations of the Napo Group (Shanmugam, 2000; Vallejo C. et al., 2021; Zuniga et al., 2021b), such indications are notably scarce in the M1 Sandstone Formation within the study area. The restricted scope of the study zone might still hold vestiges of earlier river fill upstream, possibly a result of intensified erosion from wave or tidal forces during periods of marine transgression, coupled with a paucity of fluvial sediment sources. This absence of residual river deposition is mirrored in some contemporary tide-influenced sedimentation environments, such as the Qiantang estuary (Lin et al., 2005; Zhang et al., 2014b) and the South Alligator estuary (Woodroffe et al., 1989). Given its proximity to shallow seas along the continental margin, the study area's sedimentary patterns are intricately shaped by a blend of tidal currents, fluvial currents, and wave currents, as well as local micro-structures. This complexity suggests the possibility of diverse depositional environments within the strata, potentially encompassing both fluvial and deltaic settings (Tang et al., 2019; Vallejo et al., 2017, 2021).

3. Data and methods

In this study, our dataset primarily includes core, well logging, and seismic data. The core samples serve as the most logical and effective evidence for guiding the reconstruction of ancient environments. Our analysis focuses on 13 coring wells in the T Block (Fig. 2A), where a total of 244 m of core was meticulously observed. This involved detailed descriptions of lithology, sedimentary structures, grain size, and other features to identify lithofacies types and explain environments, as shown in Table 1. We established an interpretation scheme based on petrological characteristics and facies markers, which provided a preliminary reconstruction of the paleoenvironment of the M1 sandstone segment in the central part of the Oriente Basin's Napo Formation.

To further reveal the variability in depositional processes, we adopted the method of quantifying mixed-process variability, proposed by Rossi et al. (2017). This approach involves analyzing variations in lithofacies associations among different well sections. The crux of this method is correlating the frequency of specific depositional structures with corresponding depositional processes (such as those of rivers, tides, and mono-directional waves). This is achieved through a statistical analysis of published literature that documents the genesis of sedimentary structures in multiple basins. The result is a combination of probabilities that quantitatively characterizes these complex processes. This innovative method is particularly useful in transitional systems for quantitatively analyzing mixed hydrodynamic conditions. It is valuable for assessing variations in hydrodynamic environments or in guiding predictions about environmental evolution based on sedimentary structures preserved in rocks (Peng et al., 2018; Lin and Bhattacharya, 2020).

In the study area, we utilized data from 540 wells (Fig. 2A), each equipped with complete well logging curves. These wells exhibit an irregular distribution, with a notable concentration in oil fields like D field and F field. We amassed a comprehensive collection of well logging curve data, encompassing gamma (GR), acoustic (DT), and density (DEN) curves (Fig. 2B). Our goal was to elucidate the distribution characteristics of sedimentary facies throughout the area. To achieve this, we compared the well logging response characteristics of different facies associations, using typical core well facies feature as a benchmark. We also established key sections to analyze the distribution of sedimentary facies in various directions. Based on these findings, we distinguished the boundary values of sand and mud deposits using response values of GR curves. This approach enabled us to interpret the lithology of the target intervals throughout the entire well, uncovering the spatial variation patterns of sand and mud components. Concurrently, we utilized porosity and permeability data from 493 core plug samples collected from coring intervals.

Additionally, our seismic data encompasses several major oil fields within the study area (Fig. 2C)., featuring a vertical and horizontal spacing of 12.5 m. The primary frequency of the target layer is approximately 45Hz. The seismic root mean square (RMS) amplitude attributes were used as a supplement to guide the planar distribution of sediments. By integrating sand body thickness data at well locations, we successfully characterized the planar distribution features of the sand bodies within the study area.

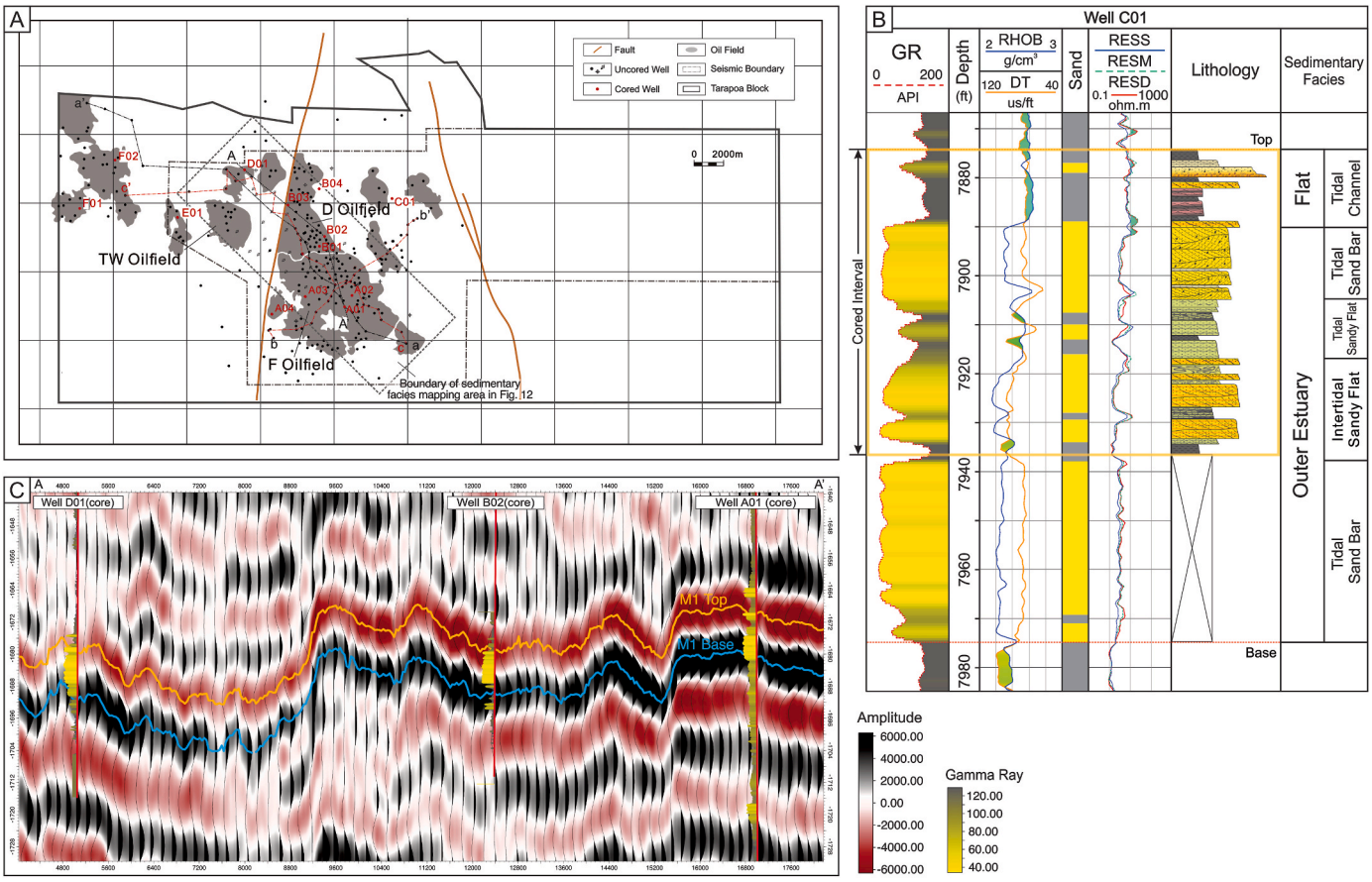

Fig. 2. (A) Location map showing wells cored and logged, seismic data and oilfields within the T Block (Study Area). (B) Example of sedimentological features in well data: logging data for Well C01, showing the logging types, lithological interpretation, and sedimentary facies interpretation. (C) The M1 Sandstone Formation on a seismic profile with three gamma ray measurements on three wells. See Fig. 2A for seismic-profile location.

4. Results

4.1. Sedimentary facies associations

Core samples reveal sediments that retain evidence of tidal or fluvial reworking to some extent. Here, we discuss in detail the sedimentary characteristics and genesis of these sediments.

By analyzing the features of core samples, we identified fourteen facies' types (Fig. 3), described their petrological characteristics, and provided interpretations of their depositional origins, summarized in Table 1. Based on the stacking patterns and genetic relationships of these facies (F), we identified seven facies associations (FA) (Fig. 4). The criteria include: 1) facies contact relationships; 2) trends in grain size and sedimentary structures; 3) sedimentological principles, such as changes in hydrodynamic conditions and succession relationships. This scheme applies to all core wells in the T block. The occurrence of these facies and facies association patterns reflects the variation in sedimentary processes within the study area. The following sections provide detailed descriptions of these facies associations.

4.1.1. Tidal channel (FA1)

Description: This facies association is mainly composed of facies 4, 5, 6, 13, and 14 (Fig. 5). The thickness of this facies ranges from 1 to 1.5 m. Lithological changes are rapid, with the base dominated by coarser sandstones and gravelly sandstones, which are poorly sorted. Upward, it transitions into fine-grained sandy and muddy deposits, exhibiting an overall normal grading. The diameter of the gravels can reach up to 1.5 cm, suspended within the sandy components to form thin gravel layers, possibly indicating lag deposits within the tidal channel. Facies Association 1 has an erosional contact with the underlying facies., showing trough cross-beddings with indistinct laminae boundaries and particles with a certain degree of orientation. The bedding types in FA1 gradually shift upward to parallel or horizontal bedding, and in some cored intervals, alternating grain sizes correspond to tidal flow influences.

Interpretation: This facies association is interpreted as a tidal channel. Lag deposits, cross-bedding, and normal grading are basic indicators of a tidal channel. The presence of coarse-grained components and cross-beddings indicates strong water energy, while unconsolidated medium to coarse sandstones suggest rapid sediment accumulation. Within FA1, further differentiation between developing tidal channels and terminal migrating tidal channels can be made. The former has coarser grain sizes and more significant tidal influence, indicated by suspended gravel interlayers and tidal rhythmites, likely located near the estuary mouth or intertidal zone (Elliott, 1986). The latter is finer grained, with fewer bidirectional flow indicators, often reflected by epsilon cross-beddings indicating unidirectional flow. The continuous mudstone deposits in facies 13 and the well-developed asymmetric climbing ripple cross-beddings suggest deposition in weak hydrodynamic conditions with a single dominant flow direction. Core observations reveal alternating brown-black colors in the muddy and silty deposits. Although direct evidence is limited, this color alternation may be related to periodic exposure, which is consistent with formation in a muddy intertidal zone. As water energy further decreases, bedding types change from climbing ripple lamination to horizontal bedding.

4.1.2. Tidal Sand bar (FA2)

Description: This facies association mainly consists of facies 2, 3, 4,

Table 1
Characteristics of the lithofacies in the M1 Sandstone (modified from Zhu et al., 2024, Facies Code referred to Zhu et al., 2024, Fig. 2).

Facies Name	Facies Code	Composition	Sedimentary features and bioturbation	Interpretation
Sandstone with wavy lamination, weak bioturbation	1 Sw	Dark-gray colored, fine- to middle-grained quartz sandstone as the main body and white colored fine to upper fine-grained sandstone as interface, featuring some extent of crypto bioturbation.	contains symmetrical crests and troughs. And each individual crest or trough is stacked together with each layer slightly offset. An integral influence of bioturbation appears on the components, as evidenced by indistinct interface.	The wavy lamination can be formed by the migration of straight ripples. The presence of distinct ripple marks indicates an association with the intertidal sand flat facies. This phenomenon typically formed in open tidal flat areas, influenced by the ebb and flood flow of tides (Jo and Choi, 2016).
Sandstone with low-angle planar cross-beddings, intraclasts	2 Sl-i	Fine- to middle-grained quartz sandstone with the appearance of reactivation surfaces, resulting in layers with varying angles of orientation. Planolites intermix with the sandy components	Low-angle cross-beddings, with angles ranging from 30 to 40° between sets of laminae. In some locations, bidirectional (i.e., herringbone) cross-stratification can be observed. The presence of bioturbation has resulted in indistinct layer boundaries.	The high energy of the water body is indicated by the variations in the direction of the bedding, reflecting frequent changes in the dominant flow direction. The uneven distribution of oil saturation suggests the influence of subtle bioturbation. The bioturbation of microorganisms modified the fuzzy internal structure and consistency of the original sediment.
Sandstone with hummocky cross-stratification, minor intraclasts	3 Sh	Dark-gray colored, fine- to middle-grained quartz sandstone with hummocky cross-beddings. Some infilling components, like Planolites, are observed.	Hummocky cross-beddings are storm-generated. Only the crests are visible as the indicators. However, the interface is fuzzy and unclear resulted by crypto bioturbation.	Hummocky cross-beddings mean the appearance of occasional storm beds. This type of stratification is deposited in locations influenced by storm waves.
Sandstone with horizontal lamination	4 Sp	White-colored, very fine-grained sandstone with extremely low porosity and permeability, and relatively thin bed thickness.	The development of horizontal bedding is on the top of a section of Facies 2 with a lack of evidence of bioturbation. And the horizontal bedding with gray color varies in the density of development.	The facies refer to the deposition that occurs during phases of reduced or minimal sedimentation in the process of tidal bar sedimentation. It represents the time intervals when sedimentation and flow slow down or temporarily cease, leading to the accumulation of sediments in the tidal bar.
Massive conglomeratic sandstone with intraclasts	5 SGm-i	Dark-gray colored, conglomeratic coarse- and middle-grained quartz sandstone with mudclasts, pyrite nodules, and fragments of amber. Poorly sorted and subrounded.	Less well-defined bedding with abundance of sandy intraclasts, many of which are oriented according to the lamination. Some conglomeratic components have large diameters up to 2 cm, floating within the sandy components.	High-energy traction processes and fine facies are eroded into sandy intraclasts. The abundance of intraclasts (many of which are layer-oriented) indicates the strength of tractional forces. And the conglomeratic components with floating condition reflect a span of water flow velocity increasing. And the gravels generally appear at the base, as channel lag deposits, corresponding to erosional features.
Sandstone with climbing-ripple cross-lamination with mudclasts	6 Scr-i	Gray-white medium-grained sandstone and white fine-grained sandstone coexist, with varying amounts of intraclasts present internally. The content of muddy intraclasts varies significantly across different grain sizes.	Alternating grain size components appear and gradually thin out laterally. Fine-grained quartz interbeds with ripple bedding is accompanied with large-size elongated muddy intraclasts. Medium-grained sandstone contain less thick, muddy intraclasts.	Partial of the climbing-ripple lamination is corresponding to the erosional surface, including elongated muddy intraclasts. The occurrence of locally developed alternating grain size components in sandy interbeds reflects the tidal influence under the hydrodynamic erosion of rivers. The scale of these interbeds can indicate the degree of tidal impact.
Sandstone with trough cross-lamination (unidirectional)	7 St	Medium to coarse-grained sandstone, light brown(influenced by hydrocarbon injection), or grayish-white colored.	Trough structure, and some core samples exhibit an unconsolidated state and fragmentation.	The coarse grain size, uneven injection, and scouring characteristics indicate strong hydrodynamic conditions, and the unconsolidated characteristics reflect the rapid deposition of sandy sediments.
Sand/shale interlaminated/ interbedded, ratio 3:1	8 I1	A higher proportion of sandy content than the mud content. The sandstone is predominantly gray, white in color, while the mudstone is gray-black. The sediment sorting is relatively good. And mudstone forms double mud drapes	This sand/shale-interlaminated/ interbedded feature is composed of thick, sandy component and thin, muddy component(≈2 mm). It exhibits typical tidal bedding characteristics, with the development of mud laminae and some soft-sediment deformation structures.	These sand/shale-interlaminated rock are called "tidalites" (Coughenour et al., 2009b). The lamina sets with alternating granulometries are inclined heterolithic stratification (IHS) that suggest tidal influence. The more sand component is contained, the stronger and longer lasting the tidal currents are, corresponding to uneven intensity of the flood and ebb currents.
Sand/shale interlaminated/ interbedded, ratio 1:1, and weak bioturbated	9 I2-b	The overall sand content is comparable to the mud content, with gray-white sandstone and gray-black mudstone. The sediment is poorly sorted and subrounded, with the bioturbation of biogenic burrows, like Skolithos.	This sand/shale-interlaminated/ interbedded feature belongs to a typical tidal heterolithic rock, with 50% sand component and 50% mud component. The sandstone forms lenticular bedding, with less lateral consistency than facies 8.	Mud and sand fractions are present in a 1:1 ratio, reflecting the balanced characteristics of tidal fluctuations in the intertidal zone. Tidal fluctuations lie at the boundary between transporting sand and mud, making it a typical feature of the intertidal zone (Webb et al., 2015). The slack water period and the tidal flow period have comparable durations.
Sand/shale with lenticular lamination,	10 I3-b	Grayish-white sandstone and grayish-black mudstone, exhibiting bad sorting resulted	Sand content is low, while the mud content is high. Wavy lamination and abundant mud drapes. It shows signs of fracturing,	The sediment is primarily composed of mud, and the presence of double mud layers and tidal rhythmites indicates the presence of a

(*continued on next page*)

Table 1 (*continued*)

Facies Name	Facies Code	Composition	Sedimentary features and bioturbation	Interpretation
ratio 1:3, and strong bioturbated		by intensely bioturbated processes, like Chondrites and indistinct bioturbation.	fragmented structures, and abundant bioturbation. The sand content has the poorest lateral continuity.	mud flat in the upper intertidal zone. As the flow energy weakening gradually, the more biological activity occurs.
Sandstone with flaser lamination and weak bioturbation	11 I4-b	White-colored, medium to fine-grained quartz sandstone with a small amount of elongated muddy clasts and localized presence of carbonaceous and micaceous fragments, and Planolites.	Flaser bedding, interbedded with heterolithic facies, bioturbated with Planolites, with syn-sedimentary deformation structures and synaeresis cracks	The sorting is good, with some locations affected by bioturbation. The presence of indistinct gray bands suggests subtle lamination. The absence of muddy components reflects the strong hydrodynamic conditions in the subtidal zone.
Sand/shale interlaminated/ interbedded, crinkled lamination, and intraclasts	12 I5-i	Grayish-white sandstone and grayish-black mudstone are comprised of soft-sediment deformation. The relative content of sandy and muddy components varies significantly vertically, and there is a noticeable variation in bed thickness.	Crinkled lamination (soft-sediment deformation) is observed, along with the presence of water escape structures. The folds exhibit significant differences in their morphology, scale, and continuity.	Crinkled lamination are likely associated with storm activity and bioturbation. However, the most plausible explanation is the influence of tidal hydrodynamics. Sudden increases in flow strength caused by bore currents can resuspend sediment and disturb previously deposited sediments, typically observed in tidal channel areas and tidal flat near river/channel mouths (Chanson, 2011; Tessier et al., 2017).
Clayed siltstone with epsilon cross-bedding and horizontal bedding	13 Secr	The lithology consists of mudstone and siltstone, with colors ranging from reddish-brown to dark gray. There are also light gray fine-grained sandstones with minor amounts of mudstone and siltstone components.	Oxidation and reduction colors can be observed in the silt and mud content, possibly due to the differences in elemental content.The sedimentary layers exhibit asymmetric ripple lamination, characterized by the presence of distinct foreset structures.	Fine grain size reflects a sustained low-energy hydrodynamic condition, while the presence of unidirectional climbing ripple lamination indicates the dominance of single-directional flow, controlled by the suspension and flocculation of clay particles. Considering the sedimentary structures and the fine-grained silty/muddy component, it indicates an environment in the upper part of the tidal zone.
Massive shale with carbonaceous clasts	14 Fm	Black mudstone, containing carbonaceous debris. Compared with laminated marine mudstone, facies 14 is more homogeneous.	Blocky bedding, with the development of fragmented fractures.	Blocky bedding of clay means the setting exhibits a slow and stable sedimentation rate. And the presence of carbonaceous debris indicates the plants growing on the supratidal zone.

and 6 (Fig. 5). The thickness is considerable, reaching up to 5–6 m. The lithology is primarily medium to fine sandstone, with slightly coarser grains at the base, and the logging curve generally presents a box shape. Internal structures are mainly composed of trough cross-beddings (wave influence?), bidirectional low-angle cross-beddings (tidal influence), and parallel bedding. These sandy deposits exhibit good porosity and permeability, and core observations indicate that they are oil saturated. Occasionally, facies 4, fine sandstone with horizontal bedding (Fig. 3d), is present, displaying tidal rhythmites, with a thickness of 5–10 cm and extremely low porosity and permeability.

Interpretation: Based on the observed sedimentary thickness, sedimentary structures, and grain size characteristics, this facies association is interpreted as a tidal sand bar, which is one of the most important deposits in estuarine setting. The continuous development of cross-beddings reflects the strong hydrodynamic conditions in the depositional environment, and the occurrence of bidirectional cross-beddings further indicates changes in the dominant hydrodynamic direction during the tidal cycle. The transition between different types of bedding is due to the varying hydrodynamic conditions during the growth of the sand bar. As the thickness of the sand bar increases, the water depth over the bar top changes continuously, leading to initially increasing and then decreasing energy acting on the bar top. This may be one reason why the internal bedding types transform from central cross-beddings to parallel beddings upward. Additionally, changes in hydrodynamic conditions are also reflected in the grain size of the sediments. The fine-grained facies 4 observed within the sand bar corresponds to tidal couplets formed during periods of weak hydrodynamic conditions between two phases of sand bar deposition. The presence of this sedimentary structure, including fine-grained components and even alternating sand-mud layers, interrupts the continuous cross-bedding typically seen in tidal sand bars, reflecting the sediment sorting effect of tidal action during phases of reduced hydrodynamic energy.

4.1.3. *Intertidal muddy flat (FA3)*

Description: This facies association mainly consists of facies 5, 10, and 14 (Fig. 5). The thickness of this facies association ranges from 2 to 3 m. The lithology is primarily very fine-grained mudstone, with thin sandy deposits (~1 cm) fully encased in muddy components, forming tidal rhythmites characterized by lenticular bedding (F10). There is clear evidence of bioturbation and biogenic burrows within these muddy facies, disrupting the continuity of the bedding (Fig. 3i). In addition to tidal rhythmites, massive mudstone (F14) deposits are of comparable scale to facies 10. Occasionally, limited-scale intraformational clastic-bearing massive sandstone (F5) is observed between the muddy facies. Unlike FA1, facies 5 in this association lacks gravel components. Physical property tests indicate that this facies association has more pronounced heterogeneity in porosity and permeability characteristics compared to the sandy facies associations (FA1 and FA2), with bioturbation likely playing a major controlling role. In bioturbated facies, porosity can reach up to 20%, while the porosity of purely muddy components is less than 10%.

Interpretation: The high proportion of muddy components in this facies association reflects formation under relatively weak hydrodynamic conditions. The presence of tidal rhythmites indicates tidal influence on the deposition of this facies association. Based on grain size characteristics and sedimentary structures, this facies association developed in the intertidal zone as mudflat deposits, where hydrodynamic conditions were restricted to a low level. Due to the abundance of muddy components, flame structures and cracks along the mud layers can be observed in the core. These pieces of evidence indicate lower water energy than facies 8 and 9, with reduced carrying capacity leading to the deposition of suspended material. In general, the degree of bioturbation and the content of muddy components are closely related to hydrodynamic strength. Environments with weaker hydrodynamics typically have higher muddy sedimentation and stronger bioturbation.

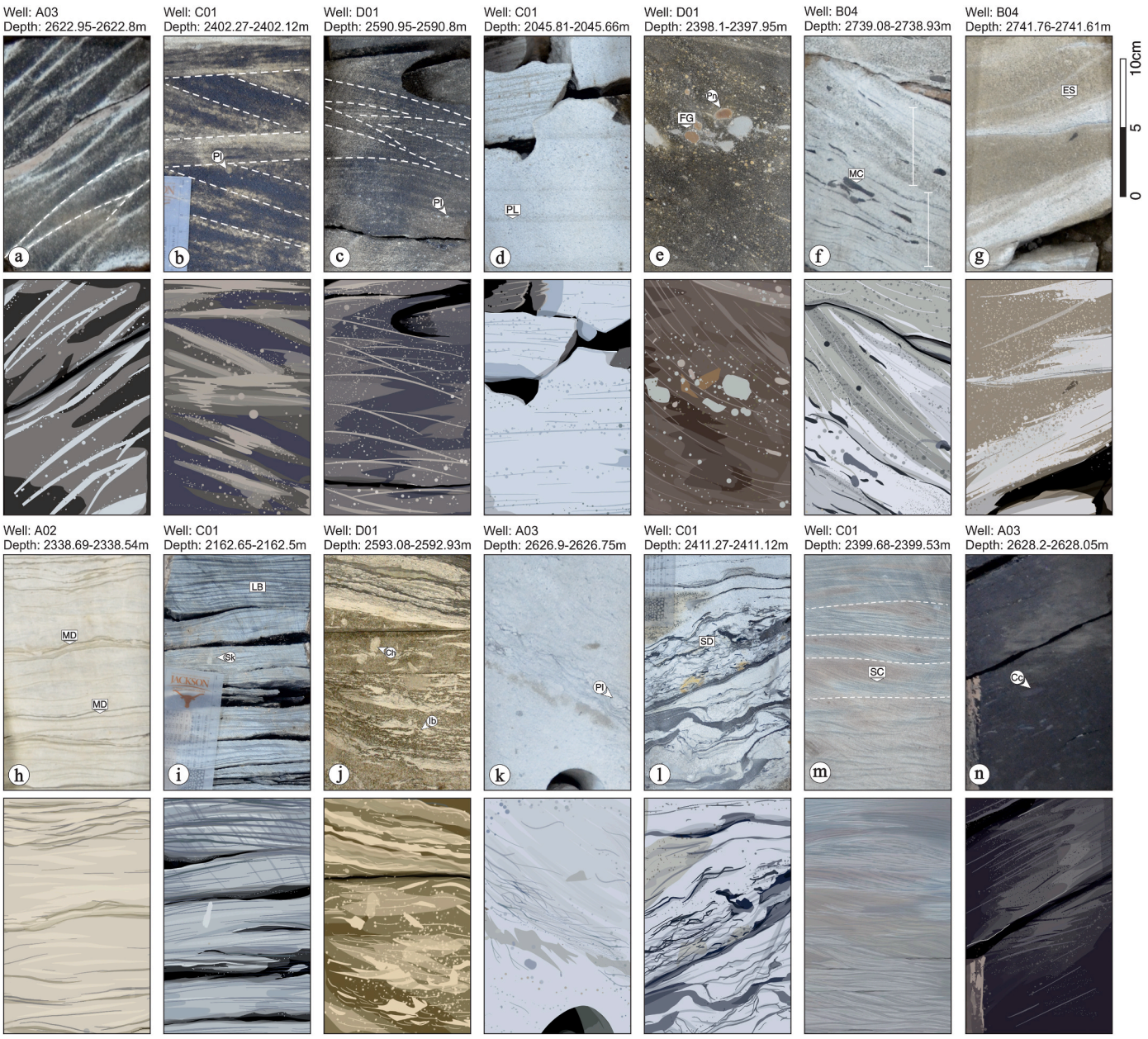

Fig. 3. Core photographs and corresponding sketches of typical lithofacies from M1 Sandstone formation, arranged in the order of facies codes in Table 1. All depths represent core depths. (a) Dark-gray colored sandstone with wavy lamination, weak bioturbation. (b) Dark-gray colored sandstone with low-angle planar cross-beddings, intraclasts, e.g. Planolites (Pl). (c) Dark-gray colored sandstone hummocky cross-stratification, minor intraclasts. (d) White-colored sandstone with horizontal or parallel lamination (PL) (e) Dark-gray colored massive conglomeratic sandstone with intraclasts, e.g. pyrite nodules (Pn) and floating gravel (FG). (f) Gray-white sandstone with climbing-ripple cross-lamination with mudclasts (MC). (g) Sandstone with trough cross-lamination (unidirectional) indicating erosional surface (ES). (h–l) Different types of tidal rhythmites with mud drapes (MD), lenticular bedding (LB), soft-sediment deformation (SD), and bioturbation, e.g. Skolithos (Sk), Chondrites (Ch) and other indistinct bioturbation (Ib). (j) Clayed siltstone with epsilon cross-bedding (SC) and horizontal bedding. (k) Massive shale with carbonaceous clasts (Cc).

(Melnyk and Gingras, 2020). Therefore, the core evidence from intertidal muddy flats exhibits different combinations of characteristics, suggesting that these sediments may be distributed over a wider area within the estuary. For example, in facies association FA3-1, the frequency of bioturbation is slightly lower compared to FA3-2, and facies 5, which reflects terminal tidal channels, appears (Fig. 5). In both cases of FA3, the variation in bioturbation intensity and muddy content suggests that FA3-1 may have developed in the intertidal zone closer to downstream zone of the estuary, where water energy is stronger. In contrast, the higher proportion of muddy components and stronger bioturbation in FA3-2 indicate that it developed in a more low-energy, upstream intertidal zone.

4.1.4. Sandy intertidal flat (FA4)

Description: This facies association mainly consists of facies 6, 8, 9, 10, 11, 12, and 14 (Fig. 5), with a thickness of 6–8 m. Facies 6, 8, 9, 11, and 12 are primarily composed of medium to coarse sandstones and fine sandstones. The sedimentary structures in facies 8, 9, 11, and 12 are related to tidal influences, including double mud drapes, wavy bedding, lenticular bedding, and soft sediment deformation structures. Additionally, in facies 6, the development of cross-beddings is characterized by cyclic changes from coarse to fine sediment components. In different

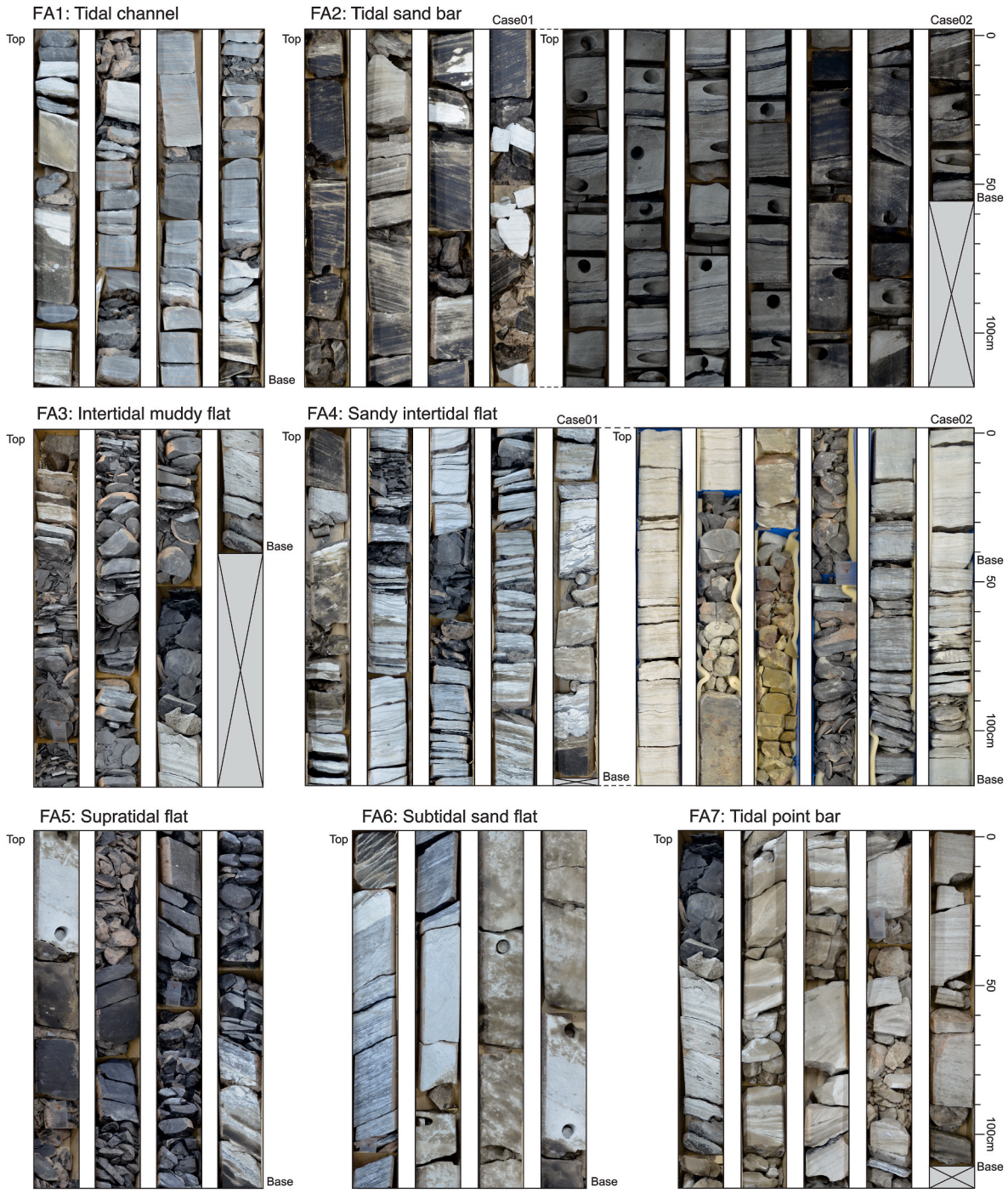

Fig. 4. Estuarine facies associations including tidal channel (FA1), tidal sand bar (FA2), Intertidal muddy flat (FA3), Sandy intertidal flat (FA4), Supratidal flat (FA5), Subtidal sand flat (FA6), and tidal point bar (FA7).

facies associations, tidal flat deposits with tidal rhythmites and tidal channel deposits with cross-beddings are commonly developed, frequently alternating. In the tidal flat facies, the proportion of sandy components is higher, and evidence of bioturbation is difficult to observe. Notably, in facies association 4-1, facies 12 exhibits soft sediment deformation, disrupting the original sand-mud inter-layered structure of the tidal flat deposits. The porosity of the sediments ranges from 25% to 30%, with indications of hydrocarbons.

Interpretation: The variations in grain size distribution and sedimentary structures among these seven facies are related to the rapidly changing hydrodynamic conditions of the intertidal zone, reflecting differences in water energy distribution between different high tide-low tide boundaries. The rapid changes in facies types effectively indicate transitions between different hydrodynamic characteristics. Therefore, considering both lithology and bedding structures, this facies association is distinguished from facies association 3, which also belongs to the intertidal zone, and is defined separately. These heterogeneous rocks, primarily characterized by tidal rhythmites, have a higher proportion of sandy components and clearer and more continuous bedding interfaces. Facies 10, 9, 8, and 11 sequentially reflect the variation in hydrodynamic energy from weak to strong. Additionally, facies 6, as evidence of tidal channels, frequently alternates with tidal rhythmites of the intertidal zone, making it reasonable to consider them together as indicators of the intertidal zone and to define facies association 4. For instance, the

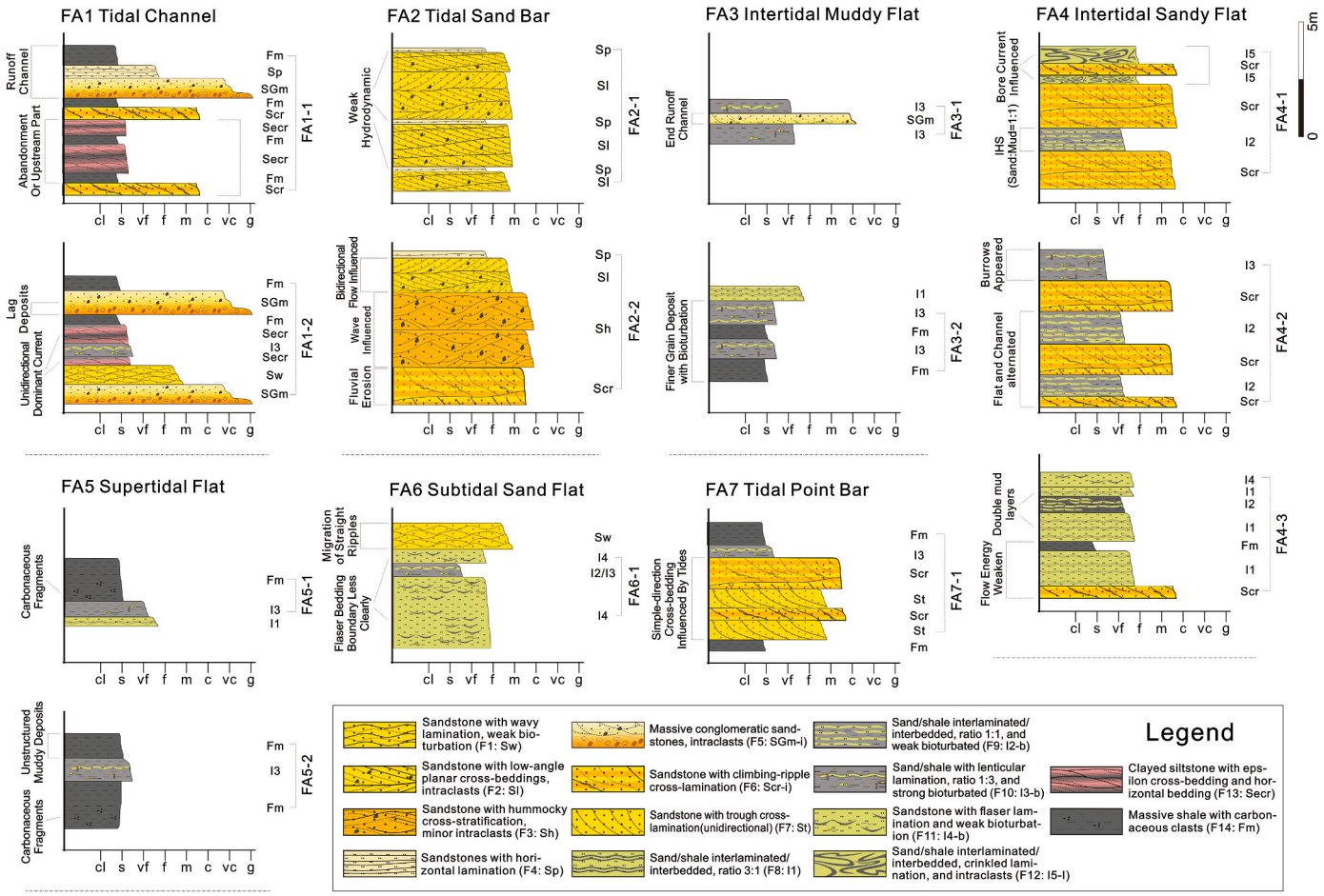

Fig. 5. Facies associations patterns corresponding to the core data. Considering the various locations within the estuarine environment, 14 types of lithofacies can be grouped into different subtypes related to various depositional processes, e.g. different flow intensity.

occurrence of facies 12, with soft sediment deformation, can be explained as a product of tidal bore-effects, where enhanced water load capacity typically occurs in low tidal flat areas. The degree of soft sediment deformation is also related to the distance from the main tidal channels of the estuary.

4.1.5. *Supratidal flat (FA5)*

Description: This facies association mainly consists of facies 10 and 14 (Fig. 5), with a thickness of 2–4 m. It is primarily a mud-dominated sequence with a high content of muddy components. Facies 14, as an indicator of the supratidal flat, is characterized by continuous mudstone with no apparent sedimentary structures. In contrast to the intertidal mudflat facies, carbonaceous detritus can be observed in the muddy facies of this association. Facies 14 can laterally transition into facies 10, with a slight increase in sandy components.

Interpretation: The supratidal flat is located above the mean high tide level, where the influence of tidal currents is minimal. The presence of structureless mudstone containing carbonaceous detritus indicates that tidal influence has reached its limit in this tidal flat region. The combination with facies 10 reflects the lateral transition from the supratidal flat to the intertidal mudflat, with an increase in tidal influence.

4.1.6. *Subtidal Sand flat (FA6)*

Description: This facies association mainly consists of facies 9, 10 and 11 (Fig. 5). The main lithology of this association is gray-white medium to fine sandstone. Facies 11 develops flaser beddings and has a large thickness, while facies 9 and 10 are characterized by lenticular beddings, bioturbation structures, and mud drapes. The thickness of the mud drapes ranges from 1 mm to 5 mm, and they contain yellow amber-like detrital particles. Tidal rhythmites are developed, with rhythmic characteristics showing alternating layers of medium-fine sandstone and mudstone. Unlike the lenticular bedding shown in Fig. 3j and k, the lithological boundaries in facies 9 and 10 of FA6 are straighter, and the sandy components exhibit larger granular structures. Additionally, Bioturbation characteristics are largely absent, with a lack of bioturbation-induced chaotic features. The discontinuities in sandy components are more likely attributed to tidal flow activity.

Interpretation: Over 90% of the components in this facies association consists of sandy deposits. The presence of flaser bedding as the main structure reflects a subtidal sand flat setting. Facies 9 and 10 is structurally more complex than facies 11. However, under the influence of strong currents in the subtidal zone, the characteristics of rhythmic bedding differ significantly from those in the intertidal zone, showing a higher proportion of sandy components overall and sandy clasts with granular features. This could be related to periodic strong ebb tides (Visser, 1980). Additionally, the mud laminae exhibit unevenly thickness, interspersed between rapidly deposited lenticular layers. Moreover, the low-frequency biogenic features observed in FA6, which decrease with increased sedimentation rate, reflects higher water energy than that of the intertidal zone. Even under relatively weak hydrodynamic conditions, the sediment grain size in the tidal bedding of this facies association reaches 1–2 mm sandy clast, indicating a relatively strong depositional hydrodynamic environment.

4.1.7. Tidal point bar (FA7)

Description: This facies association mainly consists of facies 6, 7, 10, and 14 (Fig. 5). The sediment types are primarily sandy components with ripple bedding and parallel bedding, in erosional contact with mudstone facies. The mud deposits are relatively thin, with no evidence of bioturbation. The overall thickness of this association is about 3 m. A single point bar is smaller in scale compared to a tidal sand bar, but based on core observations, both tidal point bars and tidal sand bars are multi-phase, with sand body thicknesses reaching up to 10 m. The sediment grain size is generally medium to coarse sandstone, with a vertical variation pattern of fine-coarse-fine grain size. The bedding interfaces exhibit unidirectional oriented arrangement. Additionally, in core observations, facies 6 shows abundant black mud clasts with their long axes parallel to the bedding surface, with clasts reaching lengths of 3–4 cm and thicknesses generally less than 0.5 cm. Porosity and permeability tests indicate that this facies association has higher porosity and better reservoir properties compared to other facies associations.

Interpretation: Tidal point bars are the main sand body type in the upstream areas of estuarine environments. Besides this area, this facies type generally also develops in the ebb-tidal channels on both sides of tidal flats (Jo and Choi, 2016). These regions have stronger hydrodynamics and are influenced by asymmetrical tidal flows, resulting in grain size, and bedding direction characteristics that are distinct from tidal sand bars. For instance, the grain size is predominantly sandy, but still shows rhythmic characteristics corresponding to tidal cycles, indicating that the depositional hydrodynamic environment of tidal point bars is weaker than that of the main estuary. Unlike the more uniform coarse sandy deposits of tidal sand bars, the sorting by ebb and flow tides becomes more pronounced as water flow strength decreases (Fietz et al., 2024). Since tidal point bars develop near intertidal or supratidal zones, the increased supply of mud components during deposition, combined with strong water flow, results in discontinuous and elongated mud clast deposits.

The presence of these facies types reflects the reworking of sediments by tidal currents. Considering these facies associations, the depositional period of the M1 Sandstone Formation, and the transgressive sequence background of the basin, we conclude that the study area exhibits a sedimentary development model characterized by a tidal-dominated estuarine environment.

4.1.8. Logging features of facies associations

Through detailed core descriptions, we found that different facies associations exhibit clear distinctions in terms of grain size, particle arrangement, mud content, and thickness. The GR logging response effectively records these differences (Table 2), specifically reflected in the response values and curve shapes.

4.2. Analysis of sedimentary distribution, scale, and source direction

All 540 wells penetrated the M1 Sandstone Formation. Sedimentological descriptions indicate that the M1 Sandstone Formation primarily consists of a sequence of coarse-grained sand bar sands, point bar sands, and relatively fine-grained tidal flat deposits. This predominantly sandy sedimentary sequence is stably overlying thick marine mudstone layers. The maximum cumulative thickness of the sand bodies can reach up to 36 m (~108 feet). Using a GR response value of 80 DPI as the threshold value, the logging response of 80 DPI is used to distinguish between sandy and muddy sediments. Targeting the sand bodies within the M1 Sandstone Formation, the total thickness of the sand bodies across the entire stratigraphic interval was projected onto a thickness plane map for sediment scale statistics (Fig. 6A). The sand body envelope defined by a thickness of 16 m can serve as the boundary of the main estuary. On the RMS attribute plane map (Fig. 6B), this boundary is surrounded by continuous, band-shaped low-value attribute areas corresponding to low sand body thickness zones.

The shape of the contour lines exhibits a funnel-like geomorphological pattern, with the area within well control extending approximately 20 km in a southeast-northwest direction (Fig. 6A). The sediment transportation within the estuary follows a southeast-northwest direction, consistent with the funnel-shaped mouth opening and sourced from the southeast. By analyzing the logging facies characteristics of the encountered wells, low attribute value regions near the enveloping line are interpreted as fine-grained sediment accumulation areas developing tidal flat facies. The region with sand body thickness greater than 16 m constitutes 58.1%. The extensive accumulation of sandy sediments indicates a stable sediment supply rate during the deposition period of the M1 sandstone section. Overall, estuarine sediments are well-preserved, including both marginal facies (tidal flats and runoff tidal channels) and main estuary facies (sand bars and point bars).

The distribution of sand bodies in the M1 Sandstone Formation

Table 2
Summary of the logging responses (logging facies) of the facies associations.

Facies Association	Facies Succession	Succession Interpretation	Facies (Base to Top)	Well-logging Pattern	Logging Signature
Tidal Channel (FA1)	1	Runoff channels	SGm,Sh or Se,Fh		Multiple Peak style
	2	Abandoned tidal channels	Sw,Fh,Fe/Sie		
Tidal Sand Bar (FA2)	1	Tidal bars deposited in estuary mouth zone	Sl,Sp,thin Sh		Thick trunk style, less mud response (high GR) between sand
	2	Wave current influenced tidal bar	Sw,St,Sl,thin Sh		
Intertidal Muddy Flat (FA3)	1	Intertidal muddy flat influenced by tidal currents	I3.SGm		Mainly high GR response of mud
	2	Intertidal muddy flat near the upstream zone	thin Fm,I3		
Intertidal Sandy Flat (FA4)	1	Bore current influenced flat adjacent tidal channels	Sw,I4		Higher response of thin grain size sand, mud contain up
	2	Intertidal sandy flat near fluvial-donimated zone	Sw,I2 or I3		
	3	Intertidal sandy flat near estuarine mouth zone	Sw,I1,Fh or I2		
Supratidal Flat (FA5)	1	Intertidal muddy flat near the downstream zone	thin I1,I3,thick Fm		Almost high GR response of mud
	2	Intertidal muddy flat near the upstream zone	thick Fm,I3		
Subtidal Sand Flat (FA6)	1	Subtidal sand flat dominated by tidal currents	thick Sf,thin I2 or Se		Almost high GR response of sand
Tidal Point Bar (FA7)	1	Tidal point bar deposited in tidal channels or river channels	Fm, Sp, Sw, I3, Fm		Mean sand response higher than FA2, mud appearance increase

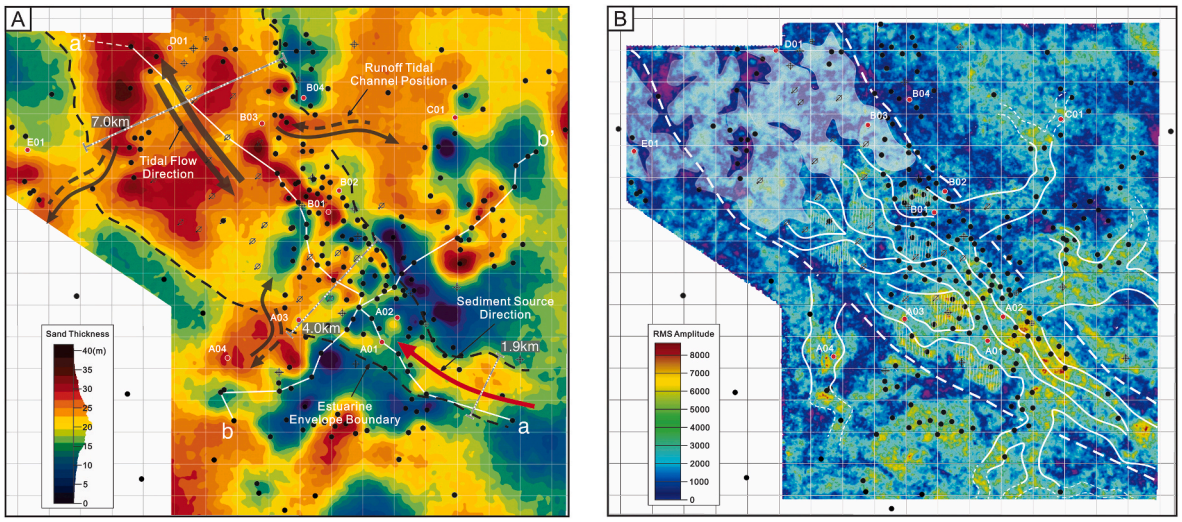

Fig. 6. (A) Isopach map of the M1 Sandstone formation covering the area of three major oilfields, D, F, and TW oilfields illustrating key paleo-sedimentary features on the source direction, contour lines of sand bodies and tidal flow direction. The contour lines exhibit an expanding trend towards the northwest. The provenance direction is from the southeast. (B) Root Mean Square (RMS) attribute map of the M1 Sandstone formation with the facies contours based on changes in attribute values. The attribute values are consistent with the distribution trend of the sand thickness shown in Fig. 6A.

represents the cumulative trend of multiple depositional periods. This trend varies along the axis of the estuary. In the relatively narrow upstream area, the distance between the two envelope lines is 1.9 km, and the distribution of sandy sediments in this area is limited, with a total thickness of less than 20 m. Core samples in this area are primarily of point bar facies, with multiple depositional units indicating that fluvial processes were the main hydrodynamic influence. In the central area where the estuary width rapidly increases (approximately between wells B01 and A01), the accommodation space for sediments increases, and the lateral continuity of sand bodies decreases. Core profiles show diverse facies association types in this area, including point bar facies and tidal flat facies. Conversely, as the estuary extends downstream, the width between the envelope lines can reach 7 km, related to the modification of estuary geomorphology by tidal action. In this area, the cumulative thickness of sand bodies can reach 33 m, almost completely covering the main estuary region. The sediments mainly consist of more extensive and contiguous sand bar deposits, as observed in the core profile of well B03 (Fig. 7).

4.3. Stratigraphy and stratigraphic framework

Detailed core descriptions indicate that the spatial distribution of deposit types within the M1 Sandstone is variable. According to the vertical changes in facies types observed in cored wells (Fig. 7) and the differences in logging features responses between adjacent wells (Fig. 8), we have divided the M1 Sandstone Formation into four major depositional periods.

4.3.1. Indicators of depositional period Division

Within the M1 Sandstone Formation, multiple secondary cyclic boundaries exist. These boundaries are related to regional relative sea-level fluctuations, accompanied by changes in facies and facies association types. The M1 Sandstone Formation is in erosional contact with the underlying marine mudstone of the Napo Shale Formation (Fig. 7). This lithological boundary is a regional marine flooding surface, resulting from a rapid sea-level rise during the initial stages of deposition. This erosional boundary is stably distributed within the study area and is comparable across the GR curve of all 540 wells. However, within the M1 Sandstone Formation, the spatial distribution characteristics of the tidal channel facies (FA1), tidal sand bar facies (FA2), tidal flat facies (FA3-6), and tidal point bar facies (FA7) reflect regional variations in the dominant depositional controls during the sedimentation process. The logging responses clearly distinguish changes in facies associations (Table 2), including the erosional surfaces of tidal channel facies. Therefore, vertical changes in depositional facies serve as critical evidence for dividing the depositional periods.

Well A01, A04, A03, and B01 are situated in the southern part of the area bordered by two east-west faults (Fig. 7). In these wells, the vertical sequences show the deposition of tidal point bar facies starting from the bottom of the M1 Sandstone interval, with thickness increasing towards the northwest. Conversely, in the upper parts of the core sections, the main depositional sand body transitions from point bar facies to better-sorted tidal sand bar facies, characterized by the appearance of bidirectional cross-bedding influenced by tidal action. The transition between tidal sand bar facies and tidal point bar facies within the estuary corresponds to different hydrodynamic conditions, reflecting differences in the depositional processes of two periods with changing hydrodynamic conditions. The strata below this interface are classified as Period01.

In Well B02 and B03, the facies types are relatively homogeneous, with tidal sand bar facies stably deposited from the top of the marine mudstone (Fig. 7). The identification boundaries of the first two sedimentary periods within the sand bar facies are difficult to distinguish further, with only a thin layer of fine-grained sandstone indicating a short-term reduction in depositional hydrodynamics. Similarly, in Well D01 and F02, located farther from the F field, the observed sand bar facies are more continuous, but the main thickness of the M1 Sandstone interval thins to about 15 m (Fig. 7). Some core sections of Well D01 show sedimentary structures formed by wave action. In contrast, Well B02 and B04 show the appearance of tidal flat facies, occasionally with point bar facies associations, at the top of the sand bar facies. This change indicates the contraction of the estuary, with tidal flat facies covering the earlier estuarine sand bars.

Along the West-East trending core section (Section F01-E01-B03-B04-C01), the frequency of facies changes significantly increases towards the sides. Tidal channel facies and tidal flat facies frequently appear, with the thickness of individual facies relatively thinning. For example, unlike the relatively continuous point bar or sand bar depositional facies in Period02 observed in the other wells, Well F01 shows smaller thicknesses for point bar and tidal flat sands, with more clearly defined depositional periods and the development of tidal flat facies. This sedimentary sequence pattern also appears in Well C01. According

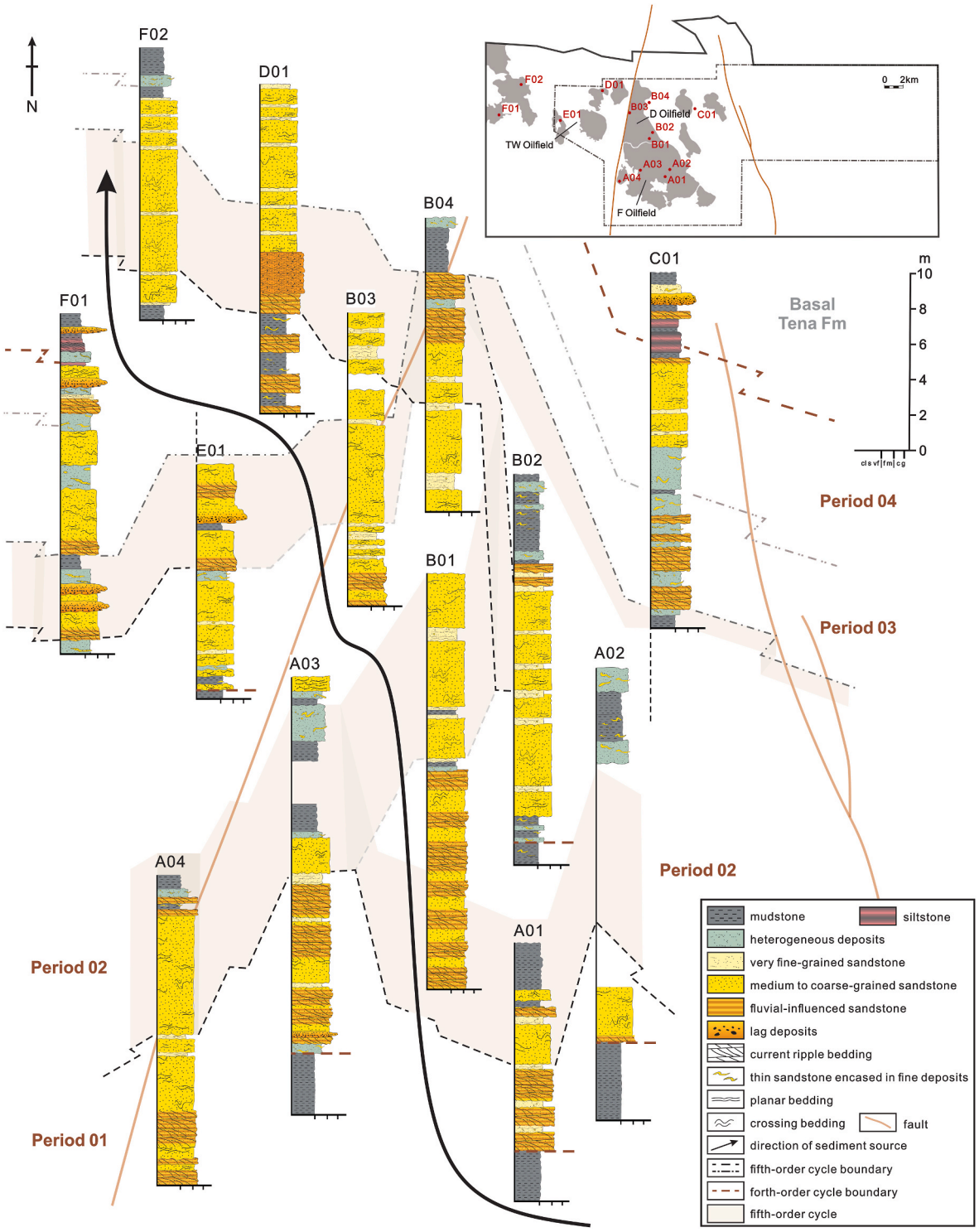

Fig. 7. Stratigraphic section(three-dimensional) of the estuary-fill succession of the M1 Sandstone formation, established from 13 cored wells. The solid arrow indicates the direction of sediment migration shown in Fig. 6A. This section shows the distribution and adjacent change of estuarine deposits. According to variations in features along the section, four sedimentary periods' boundaries have been identified.

to logging responses (Fig. 2B), the uncored interval of this well show a clear box-shaped logging curve corresponding to the continuous tidal sand bar deposition of Period01 and Period02. In the cored interval (7937-7874 feet), the facies types of Period03 and Period04 change rapidly (Fig. 2B), reflecting the rapid response of marginal facies belts to sea-level fluctuations. Additionally, the top of the M1 Sandstone Formation gradually transitions to tidal channel facies.

4.3.2. *M1 sandstone stratigraphic framework*

The sandy sediments in the M1 Sandstone Formation are characterized by large thickness and good continuity. Within this formation, three estuary-infilling periods and one open costal tidal flat period have been identified.

In each depositional sequence, the lateral comparability of logging facies reflects facies migration and changes in depositional processes. Influenced by early basement topography and water erosion, three

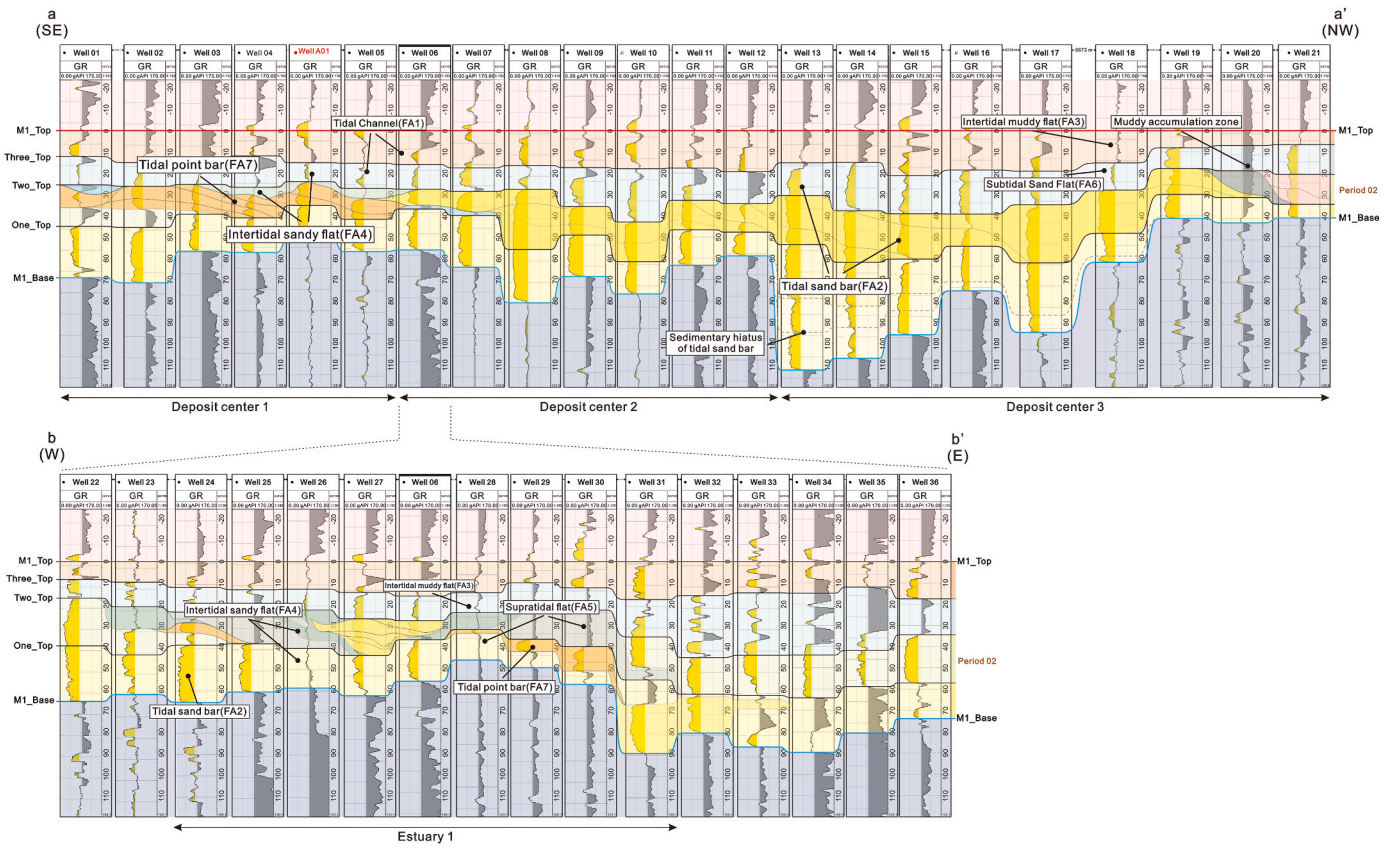

Fig. 8. (A) Cross section a-a' shown in Fig. 2A, extending from southeast to northwest (parallel to sediment migration direction). The datum is fixed at the top of the M1 Sandstone Formation according to the filling processes at different stages. Throughout the cross section, three deposit centers appear, likely related to the paleogeomorphology and sedimentary processes. Thick, continuous tidal sand bars (FA2) are distributed in the seaward direction, gradually varying to tidal point bars (FA1) with reduced thickness and exhibiting a multi-peak pattern in the well logging response. Overall, these two facies associations dominate. (B) Cross section b-b' shown in Fig. 2A, perpendicular to the central axis direction of the contour lines and intersecting with section a-a' in Well 06. The lateral facies change is evident as tidal sand bars (FA2) (near Well 27 and Well 06) transitions to tidal flat facies (FA3-6) on both sides, e.g. estuary 1 in Period 02.

depositional centers can be identified along the section a-a' (Fig. 8A). In upstream depositional center 1, sandy sediments, primarily composed of channel (tidal channel) and point bar deposits, have an average thickness of about 3 m. The low-value logging response corresponds to the thinner abandoned channel located at the top of the point bars (FA7). Depositional center 2 corresponds to the inner estuary zone, where the scale of estuarine sand bars is restricted to less than 5 m in thickness. This restriction is possibly due to sandy sediments being transported by stronger ebb currents to further downstream areas, forming a residual zone of sediments after tidal channel incision. Depositional center 3 corresponds to the outer estuary zone and is the primary area of sand body development. Sand bar deposits characterized by box-shaped logging responses are continuously developed along the profile. In this area, the sand body thickness can reach up to 10 m and shows multiple depositional phases. Due to the increased water depth in this area, the accommodation space for sediments increases, and the inflow volume increases, resulting in stronger flood currents than ebb currents. Consequently, when receiving sediments from both terrestrial and marine directions, the sand bodies in depositional center 3 are large in scale, with sand bars showing multiple depositional phases. At the farthest end, tidal sand bar deposition begins to be influenced by wave action, leading to sandy sediments being separated by thick layers of muddy deposits.

The presence of sandy sediments, distinct from the underlying marine mudstone and tidal flat deposits, signifies the rapid evolution stage of the estuary. During the initial period of estuarine evolution, the river provided substantial sediment input, leading to the development of continuous point bar sand bodies in the main channel area, which extended into the estuary and transitioned to sand bar deposits. Beyond the main estuary area, logging responses along the cross section b-b' indicate significant accumulation of tidal sand bodies in broader areas beyond the tidal flats (Fig. 8B), corresponding to some subordinate estuarine depositional zones. However, as incised valleys were filled with earlier deposits, the accommodation of the estuary decreased and remained relatively stable in subsequent depositional periods. Additionally, the estuary's development is inherited, with the main estuarine depositional area remaining relatively stable over several depositional periods. In the cross-estuary profile, a more defined estuarine outline is identified in the second depositional period. The logging facies at the envelope lines show superimposed sequences of multiple supratidal and intertidal zones, with sand bar sequences confined between the envelope lines. During the last two estuarine evolution periods, the estuary gradually filled, the thickness of sandy sediments decreased, and the logging facies transform to predominantly tidal channels and tidal point bar (Fig. 8B).

4.4. Hydrodynamic process and sediment distribution

During the different stages of the estuarine evolution, the mixed hydrodynamic intensity varies due to the differing positions relative to the shoreline and the varying degrees of estuarine evolution. Core samples have confirmed the widespread presence of tidal signals in the facies sequences, including tidal-dominated and tidal-influenced. The sedimentary structures in these rock records not only indicate the distribution patterns of ancient sediments but also preserve information about the mixed hydrodynamic conditions at the period of sediment

accumulation. The method of quantifying mixed-process variability provides a mapping scheme (Rossi et al., 2017, Table 1) for inferring paleo hydrodynamic processes from sedimentary sequences. This method reconstructs the paleo hydrodynamic signals recorded in sedimentary structures, which are complex probabilistic processes influenced by fluvial, tidal, and wave effects, revealing the energy transformation processes driving the evolution of ancient estuarine systems. By identifying the facies successions in core well sections, we applied this method to quantify the mixed hydrodynamic characteristics of ancient estuarine sediments in the study area. This effectively quantifies and visually displays the changing trends of dominant hydrodynamic processes in estuarine sedimentary sequences, revealing the impact of sedimentary processes on sedimentary distribution.

4.4.1. *Hydrodynamic characteristic changes from sedimentary structures*

After identifying and dividing the depositional periods of the M1 Sandstone Formation, we conducted a systematic analysis of hydrodynamic processes based on two core profiles oriented parallel and perpendicular to the sediment source direction. Observing the hydrodynamic distribution profile parallel to the sediment source revealed a gradual change in hydrodynamic conditions within the estuary. The base of the profile corresponds to the initial development stage of the estuary. Well A01, A03, and B01 are located near the upstream part of the estuary (Fig. 7), corresponding to the fluvial-dominated zone. The facies associations at their bases show a high proportion of fluvial influence, indicating that this area was dominated by fluvial depositional processes during the early stages of estuarine evolution (Fig. 9). Towards the shoreline along the central axis of the estuary, the influence of tidal processes significantly increases, reaching a peak tidal process probability near Well D20, with tidal energy accounting for 64% of the mixed hydrodynamic conditions (Fig. 9). The transition from fluvial-dominated to tidal-dominated energy marks a significant shift in the sedimentary facies type. The facies associations reveal extensive development of tidal flat facies and thick tidal sand bars, typical products of tidal reworking.

Further downstream, the proportion of tidal energy decreases and stabilizes around 40%, while the proportion of fluvial processes gradually increases and becomes dominant (Fig. 9). This phenomenon may correspond to the development of distributary tidal channels in this area, where sediments form tidal point bars under the influence of flood-ebb tidal currents, with sedimentary structures influenced by fluvial processes. The changes in hydrodynamic trends can be clearly visualized in the ternary diagrams for each period. By comparing the trends of each period, it is evident that tidal processes are the dominant sedimentary factors in the estuarine systems (Fig. 9). Taking Period 2 as an example, from upstream to downstream, the hydrodynamics transition from river-dominated to tidal-dominated, with wave influence appearing closer to the shoreline.

Observing the hydrodynamic ternary diagram for individual wells in the profile parallel to the estuarine axis, the vertical process probability migration curves indicate changes in environmental hydrodynamic processes. As the estuary enters the rapid development stage, the tidal component in the mixed hydrodynamics generally increases compared to the initial stage. The peak tidal intensity region migrates to Well B01 and even further upstream (Fig. 9). This pattern may be related to the further widening of the estuary's geomorphology during this period. Meanwhile, near Well D01, the probability of wave action significantly increases, reaching a process probability comparable to tidal action. This indicates that wave action penetrates the outer estuary region and becomes one of the dominant hydrodynamic forces shaping depositional features in certain local areas.

The process probability section perpendicular to the estuarine axis reflects the trend of hydrodynamic conditions changing from the center of the estuary to its sides (Fig. 10). Generally, in the central region of the estuary, tidal action is the primary hydrodynamic condition influencing tidal sand bar deposition. Comparing the lateral distribution trends of mixed hydrodynamic probability processes allows us to identify the depositional centers of the estuary. In the initial development stage's

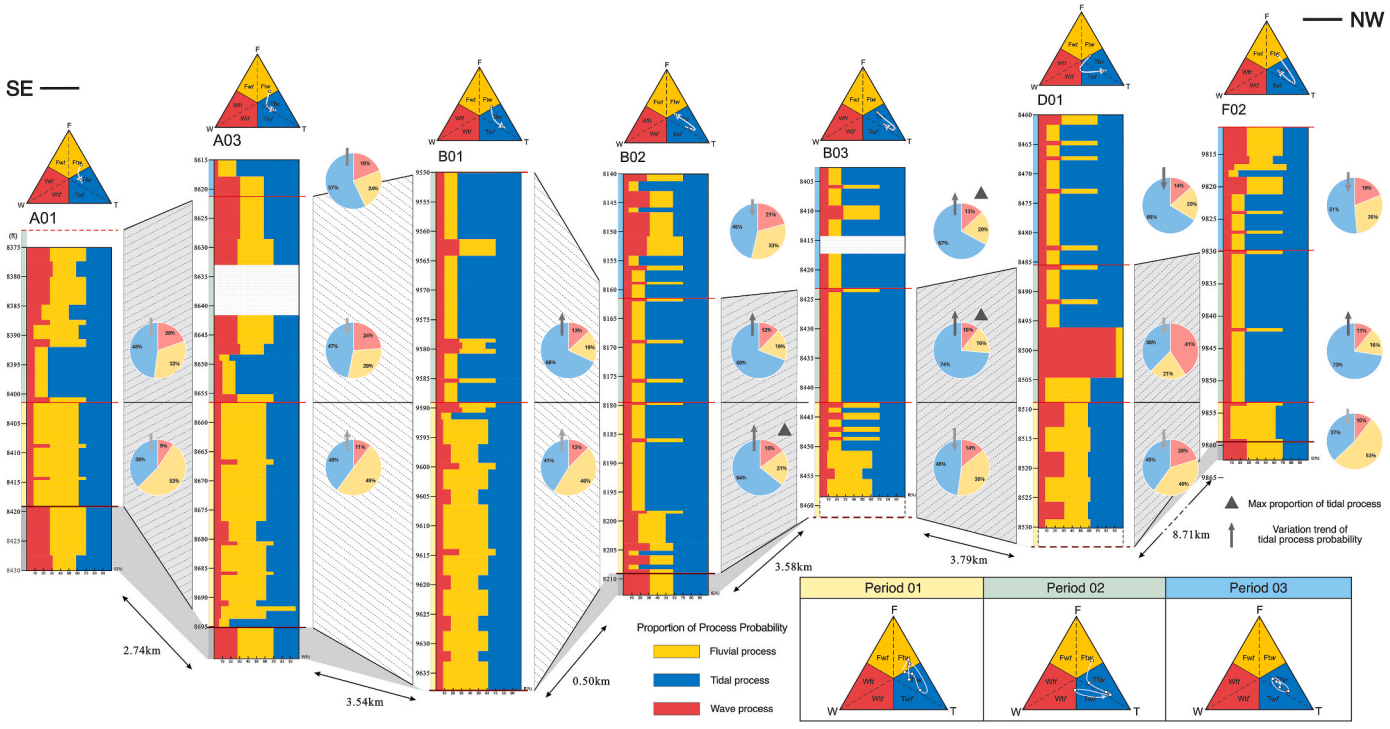

Fig. 9. Cross section of mixed hydrodynamic processes, in which core wells extending from southeast to northwest (parallel to sediment migration direction). Note that the proportion of fluvial, tidal and wave processes corresponds to the sedimentary structures of core data, shown in Fig. 7, consistent with sedimentary process probability results in shallow marine systems (Rossi et al., 2017, Table 1). In the section, the pie charts record the proportions of different processes within each single interval. The proportions are projected onto a ternary diagram to reflect the trends in process probability changes both vertically and laterally.

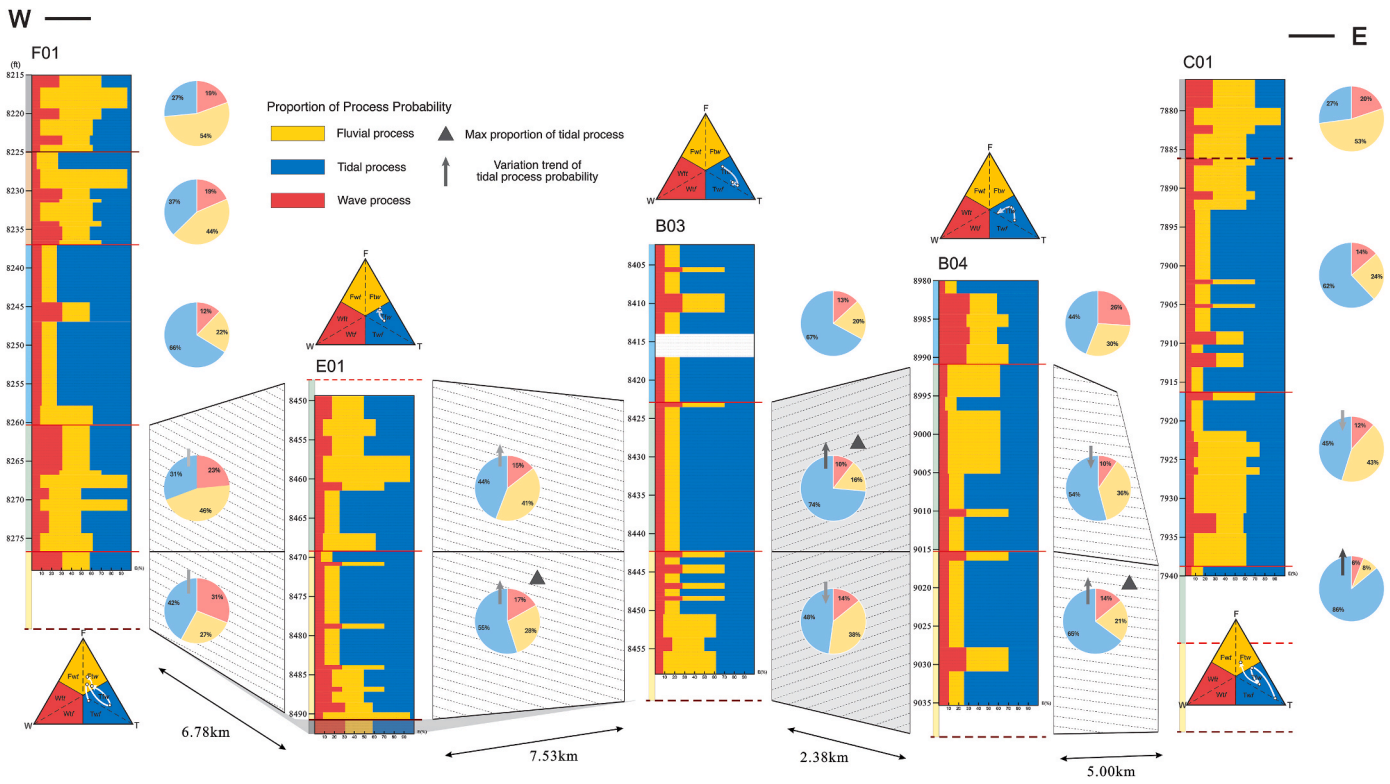

Fig. 10. Cross section of mixed hydrodynamic processes, in which core wells extend perpendicular to sediment migration direction. Note that when the cored interval is significantly smaller than the entire interval, the hydrodynamic processes may not be accurately represented.

process probability profile, there are two high tidal process probability areas on either side of well B03, possibly indicating the presence of two estuarine systems during this period. Meanwhile, a transient fluvial process is observed at the bases of Well B03 and E01 (Fig. 10), gradually transitioning to tidal-dominated processes as the estuary evolves. In the rapid development stage of the estuary, a peak tidal process probability is only present near Well B03, corresponding to the maximum water depth region of the estuary during this period. Concurrently, the strength of fluvial action increases with shallower water depths. Given that tidal-dominated estuaries generally exhibit a gradual growth trend, this characteristic of lateral hydrodynamic process change is preserved in the profile perpendicular to the sediment source.

4.4.2. *Sediment distribution under hydrodynamic constraints*

Mixed hydrodynamic processes play a crucial role in the evolution of estuarine settings, impacting sediment redistribution, facies successions patterns, estuarine geomorphology, and even influences subsequent diagenesis (Estupiñan et al., 2010). The redistribution of these sediments—through deposition, transportation, and erosion—is closely linked to local hydrodynamic conditions. Consequently, the distribution of sedimentary facies maintains a high degree of consistency with the changing trends of mixed hydrodynamic processes in the estuary (Harris, 1988; Chaumillon et al., 2010; Ekwenye et al., 2017).

As sediment transport and erosion processes continuously occur, the estuary's morphology remains in dynamic evolution. In this process, different areas of the estuary are continually filled or eroded, causing changes in local water depths and thereby influencing the relative proportion of water energy in mixed hydrodynamic processes. The absolute strength of water flow also controls sediment and facies distribution. Sediment distribution is controlled by both the absolute energy of the flow and the mixed hydrodynamic processes. This is reflected in the varying distribution of grain size and sedimentary structures within the depositional sequences. Therefore, in analyzing sediment distribution, we categorize sediments reworked by mixed hydrodynamic processes into sandy components, muddy components, and heterogeneous rock components with tidal signals. As bedload components, sandy sediments correspond to areas with the highest water carrying capacity and stronger water energy. Heterogeneous rocks and muddy components are fine-grained sediments corresponding to areas with weaker water energy. However, heterogeneous rock components experience more intense tidal reworking, indicating relatively stronger tidal influence compared to muddy components.

By establishing hydrodynamic distribution profiles of the estuary, we selected 39 non-cored wells in both parallel and perpendicular directions to the sediment source to explore sediment distribution patterns (Fig. 11A). The core wells used in hydrodynamic characteristic analysis were projected onto these two profiles. Overall, throughout the evolution of the estuary, the proportion of sandy components in the total sediment is quite high. For example, in the profile parallel to the sediment source, the average sandy component reaches 73%. However, due to the relationship between sediment distribution and hydrodynamic processes, the development scale and frequency of occurrence of the three sedimentary components vary significantly across different areas.

In the profile parallel to the sediment source, three depositional centers can be observed. The first depositional center is a tidal-dominated high-energy region corresponding to the outer estuary zone (8.5–20 km) (Fig. 11A). This area develops tidal sand bars, which are the main accumulation sites for sandy sediments. The sand bodies are large in scale, lithologically homogeneous, and lack fine-grained interlayers. The second depositional center is the energy mixing zone (6–8.5 km). The thickness and scale of sedimentation is smaller than that of the outer estuary zone but still predominantly sandy, with muddy components appearing in the later stages of evolution. This area is located on the inner side of the estuary and is a transition zone where tidal influence shifts to fluvial influence. The deposition rate of sediments is limited due to the combined effects of fluvial and tidal actions. The third depositional center is a fluvial-dominated low-energy region corresponding to the inner estuary zone (0–6 km). In this area, sediments have

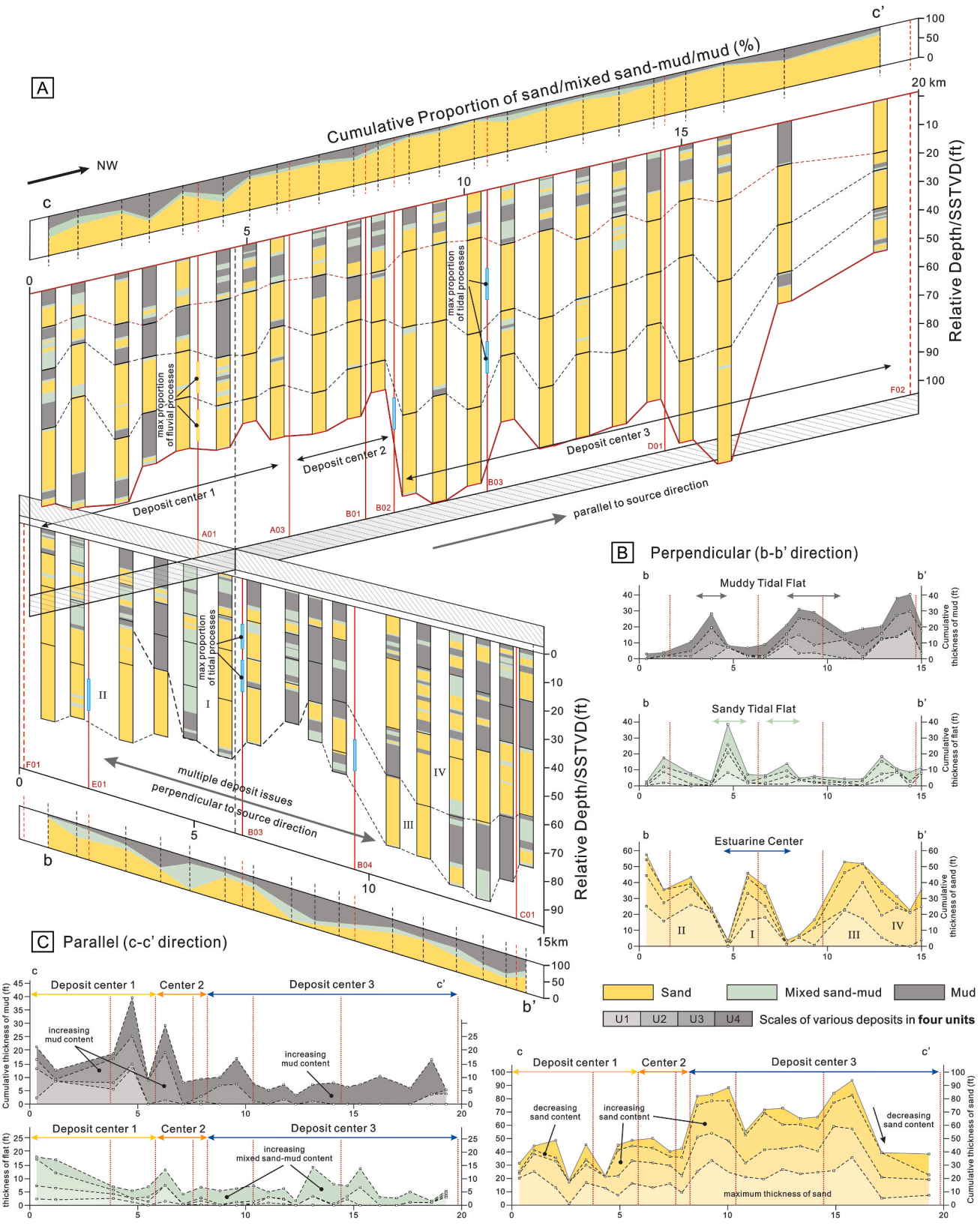

Fig. 11. Quantified sand, flat, and mud distribution data for estuarine-fill sediments in the M1 Sandstone Formation. (A) Cross section c-c' and cross section b-b' with sediment thickness obtained from GR (Gamma Ray) logging data, cumulative proportion of sedimentary contents, and the position of max proportion of tidal/fluvial processes at core wells. Note that the locations of the core wells are determined by projecting them along the direction of the section. See Fig. 2A for cross section location. (B) Thickness statistics of mud, tidal flat, and sand components in cross section (b-b') vertical to source direction. (C) Thickness statistics of mud, tidal flat, and sand components in cross section (c-c') parallel to source direction.

characteristics of fluvial environments, mainly consisting of tidal point bar facies and tidal flat facies. The increase in fine-grained sediments reflects the weakest absolute hydrodynamic intensity in this area. However, the development of heterogeneous rock components indicates that tidal processes still penetrate this region. These centers correspond to three zones of mixed hydrodynamic processes. As hydrodynamic processes determine facies distribution, these areas display marked differences in the scale of sand-mud components, facies associations, and lateral continuity.

In the section perpendicular to the sediment source, the sediment distribution trend is consistent with the distribution trend of the water body structure. Sandy components preferentially fill the deepest parts of the estuary, predominantly influenced by tidal action. As the water body becomes shallower, it transitions to heterogeneous rock components and muddy components towards the sides, corresponding to the facies transition from tidal sand bar facies to marginal tidal flat facies. During this process, the content of fine-grained components gradually increases, while the content of sandy components decreases (Fig. 11B). This sediment accumulation trend appears multiple times in the profile, most typically near Well B03. This area consistently maintains the maximum depth during the continuous evolution of the estuary, corresponding to the sedimentary center of the estuary. The central area forms uniform-grained, large-scale tidal sand bar deposits, flanked symmetrically by tidal flat deposits on both sides. This typical sediment stacking trend enables us to identify multiple estuarine units within the M1 Sandstone Formation (Fig. 11A). Nevertheless, the highest proportion of tidal influence consistently identifies the main sand body deposition area in the estuary. The tidal influence gradually diminishes towards the margins and upstream areas, a trend attributed to the attenuation of tidal energy due to bottom friction and decreased water depth from topographic changes (Dalrymple et al., 1992; Dalrymple and Choi, 2007).

Across the three periods of estuarine evolution, the sediment components show a trend of increasing sandy content and decreasing muddy content towards the sea (Fig. 11C). However, the statistical values of sediment thickness distribution across different depositional periods reveals certain differences. Among them, comparing three intervals shows that the fluctuation in sediment thickness is greatest during the initial stage of estuarine evolution; it gradually decreases during the rapid development stage and the final stage of estuarine evolution (Fig. 11C). This trend indicates the impact of valley topography on the sediment filling process during the early development of the estuary. As the early valley topography is gradually filled with sediments, the bottom of the estuary forms a relatively flat topography, and a relatively stable estuary region is gradually established. In the final period, sedimentation rate decreases, and the proportions of various grain size components are relatively equal (Fig. 11B and C). During this period, the estuary is completely filled with sediments, and the facies are predominantly fluvial facies, tidal channel facies, and tidal flat facies. In the profiles in both directions, the sediment component distribution trend lacks clear regularity. This significant difference in sediment distribution indicates that in the final stage of estuarine evolution, as the estuary is gradually filled, the depositional environment undergoes a transformation to tidal flat.

5. Discussion

5.1. Sequence-controlling factors of M1 sandstone formation

5.1.1. Persistent tectonic subsidence

Persistent tectonic subsidence provided geological conditions that facilitated the marine-fluvial transitional environment at the edges of the basin. The Oriente Basin experienced moderate geodynamic changes during the Cretaceous period (Litherland, 1994; Baby et al., 1999; Horton, 2018). During this era, the basin's tectonic shift pattern evolved from the half-graben system, established during the rift development phase before the early Cretaceous, into a state of persistent mild subsidence, under the continued influence of extensional forces (Vallejo et al., 2009; Gutiérrez et al., 2019; Jaillard, 2022). With the abandonment of Ecuadorian-Colombian margin plate subduction during the period of accretion of allochthonous terranes (~140 Ma-120 Ma), the oblique accretion and roll-back of the residual plates prompted prolonged compressive effects, leading to tectonic, a phenomenon evidenced by basic magmatic eruption events spanning the central corridor of the Oriente Basin (Albian (110 ± 5.2Ma) to Campanian (82.2 ± 2.0Ma)) (Fig. 12B) (Barragán et al., 2005; Avellaneda-Jiménez et al., 2020). Compressive reversal near the continental margin (close to the eastern cordillera) induced uplift and erosion, corresponding to a 20 Ma sedimentary hiatus, and formed a regional unconformity at the base of the Hollin Formation. Then, persistent subsidence at the basin's edges and central areas created the necessary accommodation space for the accumulation of Cretaceous clastic sediments. Accompanied by Cretaceous subsidence, the accretion of oceanic terranes beginning in the Santonian triggered several events of collision and regional uplift in the Ecuadorian margin, explaining the low subsidence and a series of sedimentary hiatuses during the Late Cretaceous (Jaillard, 2022). From the Albian stage to the Paleogene, this persistent subsidence was comparatively mild, maintaining a stable and slow subsidence rate at the eastern edge and central area of the basin (average rate of 9 m/Ma) (Thomas et al., 1995; Horton, 2018). Well statistics' subsidence curves indicate that the subsidence rate at the eastern edge of the study area was slightly lower than at the basin center (Fig. 12A), creating a gentle and broad slope zone. Constrained by the tectonic background, the extensive gentle continental shelf area, stretching north-south along the basin edge, offered open water conditions favorable for the development of depositional environments such as estuaries and other clastic coastal settings. Considering the significant sea-level rise during the Campanian period (Haq,2014), the M1 Sandstone Formation continued to progress toward the central area along the gentle slopes of the eastern basin eastern (Fig. 12B). Subsequently, this steady subsidence process transitioned to rapid accumulation between 70 and 60 Ma, likely correlating with the initial shortening of the basin during the Maastrichtian-early Paleocene (extending southward from the central Cordillera of Colombia to the eastern Cordillera of Ecuador) (Horton, 2018).

5.1.2. Sea-level fluctuations near the shoreline

Amid tectonic subsidence throughout the basin, the movement of clastic rock sediments toward the basin's center was influenced by relative sea-level fluctuations. The sequence of layers comprising black shale, bioclastic limestone, and shallow marine clastic sandstone (Fig. 13) suggests that during the Cretaceous period, the main subsidence zone of the Oriente Basin hosted a shallow continental marine environment (Jaillard et al., 1996; Baby et al., 2004). Although the Campanian depositional period was characterized by an overall regressive setting, the basin was influenced by the Andean orogeny, shifting from extensional to compressional tectonics, which caused the sea level in the study area to show a relative rising trend. (Ray et al., 2019; Vallejo et al., 2021). The sedimentary record from the latter period includes two clastic depositional sequences, the M2 Sandstone and M1 Sandstone Formations (Fig. 13). These formations represent two sets of third-order transgressive system tracts (TST), succeeded by shorter intervals of regressive events (Gutiérrez et al., 2019). Detailed analysis of the depositional traits of the M1 Sandstone Formation shows that the relative sea level rise facilitated the extensive development of estuarine sedimentary systems beneath the gentle ancient shoreline tide, ensuring sustained and expanded accommodating space. Concurrently, the relative sea level rise influenced tidal hydrodynamics, pushing the tides further upstream to the land, and creating optimal zones for trapping sandy sediments in early incised valley formations. As the relative sea level rise trend abated and the estuaries progressively filled with clastic materials, the sedimentary environment transformed significantly, with expansive tidal flat environments supplanting the original estuarine settings.

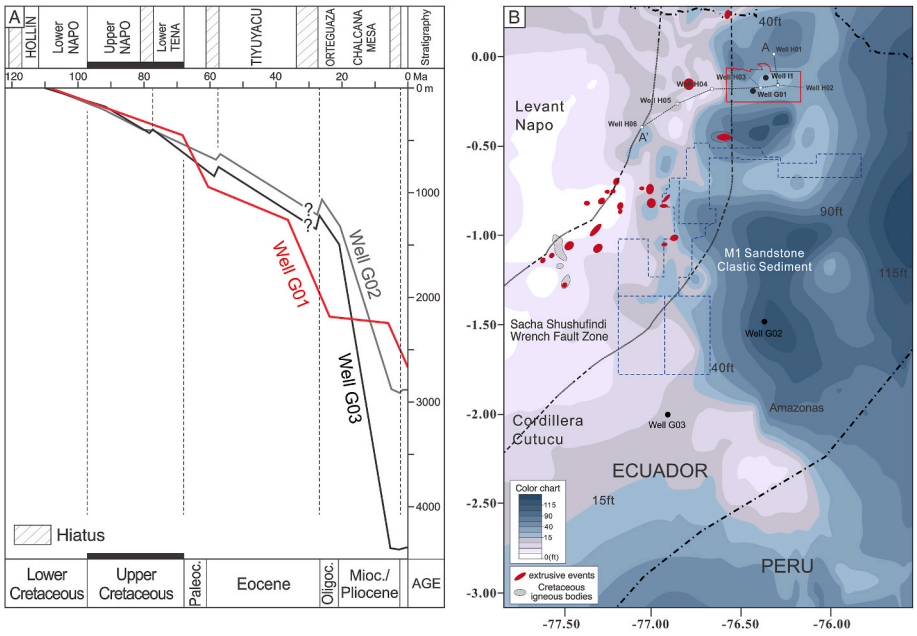

Fig. 12. (A) Sedimentary accumulation in the Oriente Basin since the base of the Napo Formation (modified from Zhongzhen et al., 2021a,b; Jaillard, 2022). See Fig. 12B for three well locations. (B) Stratigraphic thickness of the M1 Sandstone Formation in the Oriente Basin with the location of extrusive events and igneous bodies (modified from Baby et al., 2004; Barragán et al., 2005).

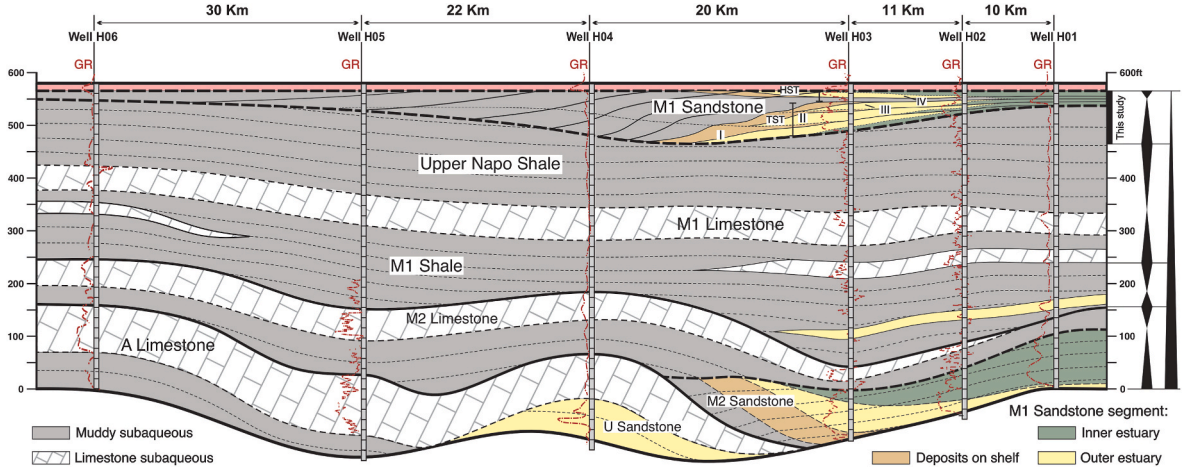

Fig. 13. Late Cretaceous sequence stratigraphic section of the northern Oriente Basin based on logging data (curves from Baby et al., 2004).
Note three evolutional stages of estuarine settings correspond to transgressive systems tract (TST) and one evolutional stage of open coastal flat setting corresponds to highstand systems tract (HST).

Estuarine environments are highly sensitive to changes in sea level, which are immediately reflected in sediment composition and depositional structures due to rapid fluctuations such as storm surges or seasonal tidal variations (Hori et al., 2002; Dalrymple and Choi, 2007; Ghosh et al., 2009; Yan et al., 2020, 2024; Yan et al., 2024a,b). Sea level oscillations affect the water depth in the transitional zone between sea and land, directly influencing the mixed hydrodynamic conditions within the estuary (Dalrymple et al., 2011; Tessier et al., 2012a; Strasser, 2018). Sea-level variations modify the original hydrodynamic conditions, thus altering water flow velocity, sediment supply, and deposition rates, which in turn reshape estuarine geomorphology (including tidal channel width and tidal sand bar scale, among others) (Kostaschuk and Best, 2005; Dalrymple and Choi, 2007; Tessier et al., 2012a; Yan et al., 2024a,b). In tidal flat areas, sea-level fluctuations lead to changes in the areas of submersion and exposure of the flats (Dalrymple et al., 1991; Yang et al., 2005; Desjardins et al., 2012a,b). Given the periodic nature of tidal action, alterations in water depth shift the positions of high and low tide lines, directly impacting the development locations of the supratidal, intertidal, and subtidal zones (Fig. 14A) (Hoekstra et al., 2004; P. R. Desjardins et al., 2012a,b; Dalrymple, 2021). These changes prompt trends in particle size, depositional structures, and bioturbation distribution in tidal flat areas to extend in landward or seaward directions (Dalrymple, 1992; Daidu et al., 2013; Zhou et al., 2021). These sediments, extensively reworked by tidal and other hydrodynamic forces, exhibit distinct differences in rock components and depositional structures, forming cyclic patterns that reflect the short-term changes in water depth (Nio and Yang, 1991).

Quantitative analysis of sea-level fluctuation amplitude shows that multiple short-term sea level rise and fall cycles (less than 3 Ma) occurred simultaneously, primarily driven by climatic and glacial events (glacio-eustasy) (Ray et al., 2019). Against the backdrop of sedimentary conditions along a gentle shoreline tide, rapid sea-level changes emerge

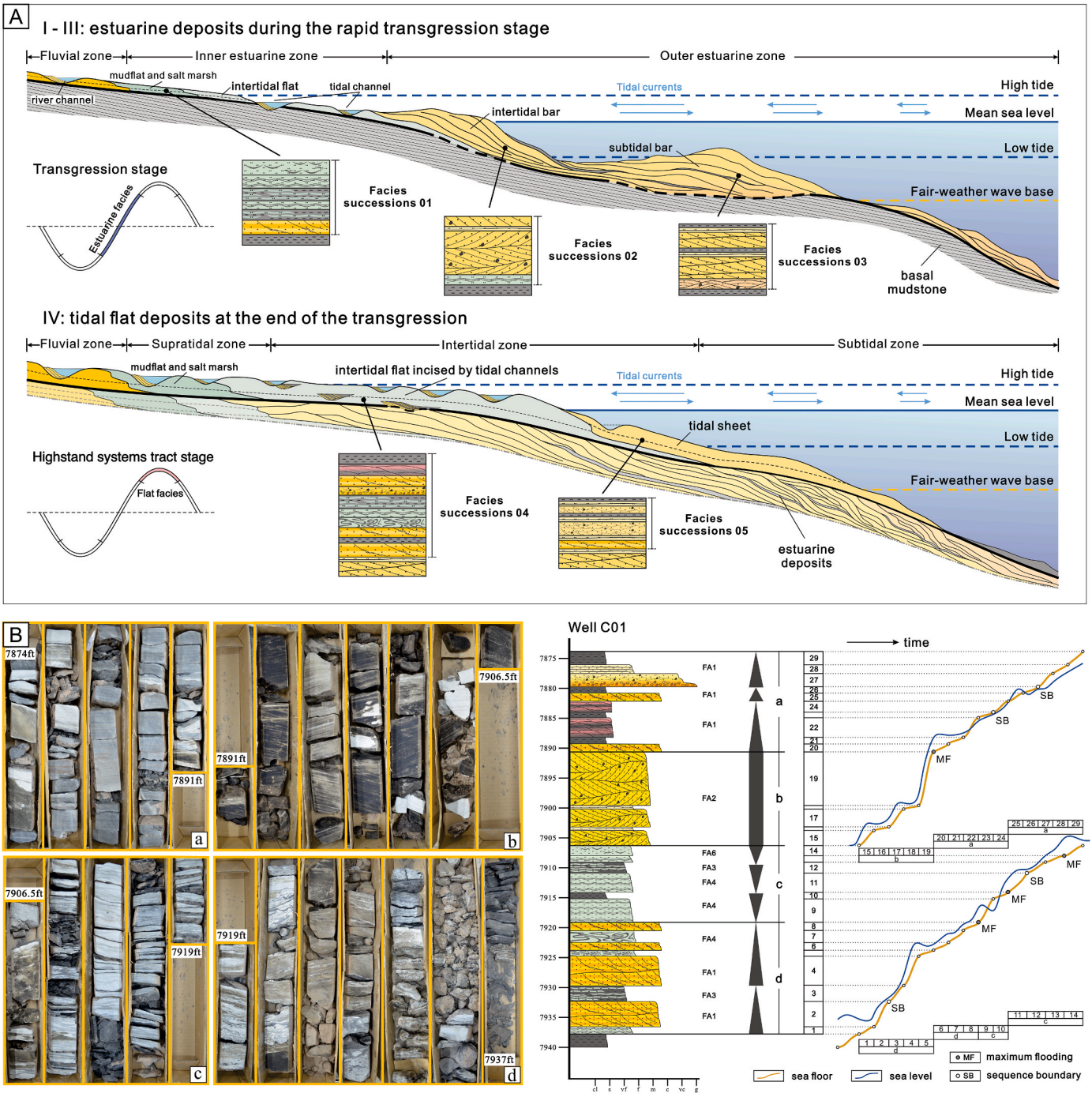

Fig. 14. (A) Schematic diagram showing sediment distribution between sea-level fluctuations controlled by tides in tide-dominated estuary and open coast tidal flat. Note the distribution of facies sequences corresponds to the mixed hydrodynamic processes between different sea-level positions. (B) Core photographs of full cored interval of Well C01. (C) Sea-level change trends reflected by sediment types in tidal coastal settings. Note that this trend curve reflects short-term fluctuations in sea level rather than long-term changes.

as a significant factor influencing depositional cycles through lithofacies sequences, exerting direct control over sedimentary environments and the extent of facies migration (Fig. 14A) (Baby et al., 2004; Jaillard et al., 1996; Jaillard et al., 2005). Core data from the study area reveal that Late Cretaceous marine transgression events created accommodation space for the ongoing accumulation of estuarine sediments. The accumulation and transport of these clastic components were confined to the coastal-transitional zone dominated by rapid sea-level changes (Fig. 14B). In conditions significantly influenced by tidal action, rapid sea-level fluctuations affected the configuration of mixed hydrodynamics, leading to complex tidal lithofacies stacking sequences (Fig. 14A) (Yoshida et al., 2007; Coughenour et al., 2009a; Ainsworth et al., 2011). Therefore, ancient estuarine sediments capture short-term facies changes due to rapid sea-level fluctuations and document significant adjustments in sedimentary environments under a continuing trend of sea level rise.

5.1.3. *Stable material source*

Stable and continuous sediment transport positively influences the evolution of estuarine environments. U-Pb geochronological results

provide a basis for analyzing the origins of the clastic components in the study area. Previous studies have shown that during this period, the Oriente Basin was not yet influenced by the Andean orogeny; its sedimentary deposits were primarily derived from the erosion of cratonic basement rocks from the eastern Guyana shield (Fig. 15A) (Horton, 2018). By reevaluating the U-Pb geochronological data of the M1 Sandstone Formation (Gutiérrez et al., 2019; Lin, 2020; Vallejo et al., 2021), the peak ages of the samples predominantly align with four pre-Andean source areas: 900–1300 Ma, 1300–1550 Ma, 1550–1800 Ma, and 1800–2150 Ma (Fig. 15B). These active peak responses suggest that the basin had a relatively abundant material supply during this period, ensuring high sediment availability for the formation of the clastic system.

However, when these samples are divided and analyzed statistically by different regions and stratigraphic sections, the peak distributions exhibit detailed variations. For instance, compared to samples from the northern T block (Study Area), samples from the eastern ITT block show no peaks before 1400 Ma and exhibit fluctuating peaks around the age limits of 950 Ma and 2200 Ma (Fig. 15B). Additionally, samples from the RNJ Province display a bimodal pattern (Fig. 15B). The variability in U-Pb age distributions among these samples might indicate the existence of two or more sediment transport pathways in this stratum. Moreover, the peak age distributions characteristics in the central area of the basin can be correspondingly found in the T Block and ITT Block. This suggests that in the more distal shallow marine shelf region, sediment mixing occurred during the continuous transport toward the basin center due to the reworking of waves and other oceanic currents. Conversely, examining different stratigraphic sections of the M1 Sandstone Formation within the study area, the U-Pb age distribution characteristics of the samples from the upper, middle, and lower parts are strikingly similar (Fig. 15C). This consistency indicates that during the rapid development of the estuarine sedimentary environment, the captured sediments were sourced from the same diffusion system.

5.2. Paleogeographic reconstruction evidence of M1 sandstone formation

5.2.1. Migration processes of estuary-dominated deposits in T block

The sediment distribution in tidal-dominated estuaries varies across different stages of evolution. We established a sand body thickness distribution map and a sedimentary facies plan for Unit II to discuss the development characteristics of estuarine sediments in T Block (Fig. 16). We identified and delineated four evolutionary periods of Estuary Unit II. These periods correspond to the initial development stage of the estuary, the rapid filling stage, the decline (slow filling) stage, and the development stage of open coastal tidal flat.

The first two stages experienced rapid transgression, during which the relative sea-level rise gradually intensified tidal influence. This is reflected by the expansion of the tide-dominated area and the contraction of the mixed zone in the landward direction(Fig. 16). During this period, sand bodies preferentially filled multiple secondary estuarine deposition centers controlled by paleotopography, eventually adjusting into a single main estuarine deposition zone. The estuary widened, with the width between its enveloping lines reaching up to 7 km, and tidal flat were distributed on both sides of the estuary. This distribution trend of estuarine facies persisted through the decline stage (Period 03). Starting from this period, the rate of relative sea-level rise became more gradual regionally. Beyond the limited energy mixing zone, the facies quickly transitioned to fluvial-dominated regions. The upstream narrow channel belt was surrounded by extensive tidal flat areas. In the final stage, sediment thickness was significantly lower than during the estuary's development stage. Sediment distribution featured a combination of upstream tidal flat facies dissected by tidal channels and downstream continuous thin sand layers (possible sand sheets). This sediment distribution indicates that as the estuary was filled, it maintained a relatively uniform low-accommodation state laterally. It is worth noting that, although evidence indicating an early fluvial-incised valley system is lacking in the study area, this does not affect the interpretation of the M1 Sandstone Formation as representing a complete third-order cycle.

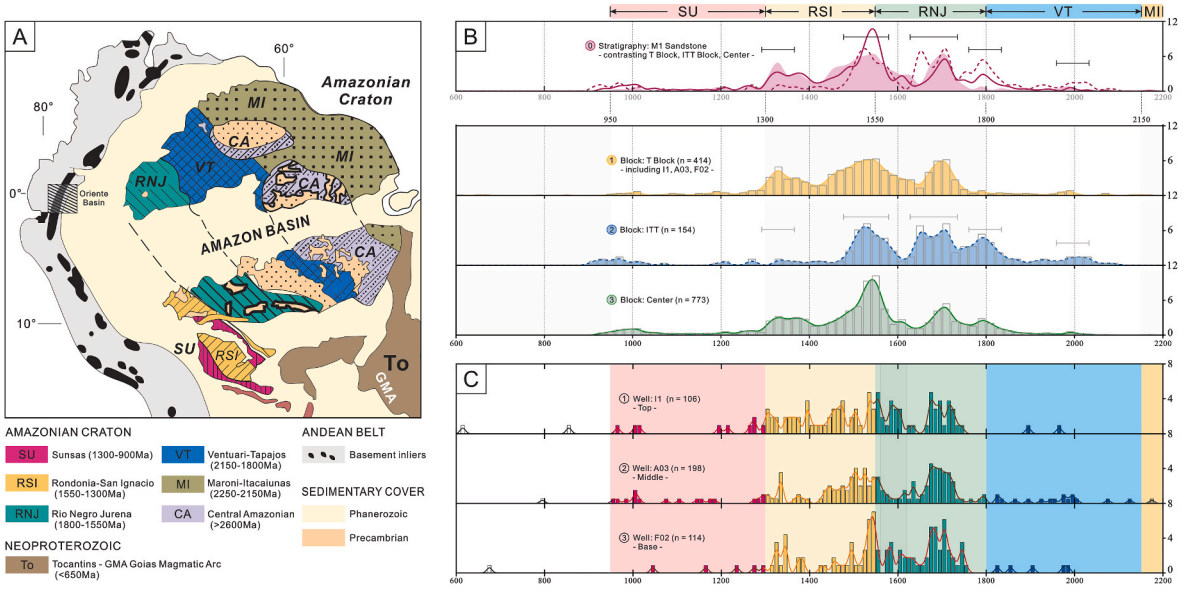

Fig. 15. (A) Sketch map showing the distribution of the Geochronological Provinces and the main lithological associations of the Amazonian Craton, north of South America (modified from Tassinari and Macambira, 1999). (B) Age histograms and probability density functions of three locations in Oriente Basin showing detrital zircon U-Pb age distributions for the M1 Sandstone Formation. The data in Diagram 0 represents a cumulative counts of the data in Diagrams 1–3, reflecting the differences in age distribution (detrital zircon U-Pb age data are from Ruiz et al., 2007a,b; Lin, 2020; Vallejo et al., 2021). See T Block, ITT Block, Center Block in Fig. 1A. (C) Age histograms and probability density functions of three wells in T Block. Note that the samples on each well are from different depth. The samples from Well I1 are taken from the top of the M1 Sandstone Formation, those from Well A03 are from the middle part, and those from Well F02 are from the base. See the location of Well I1 in Fig. 12B.

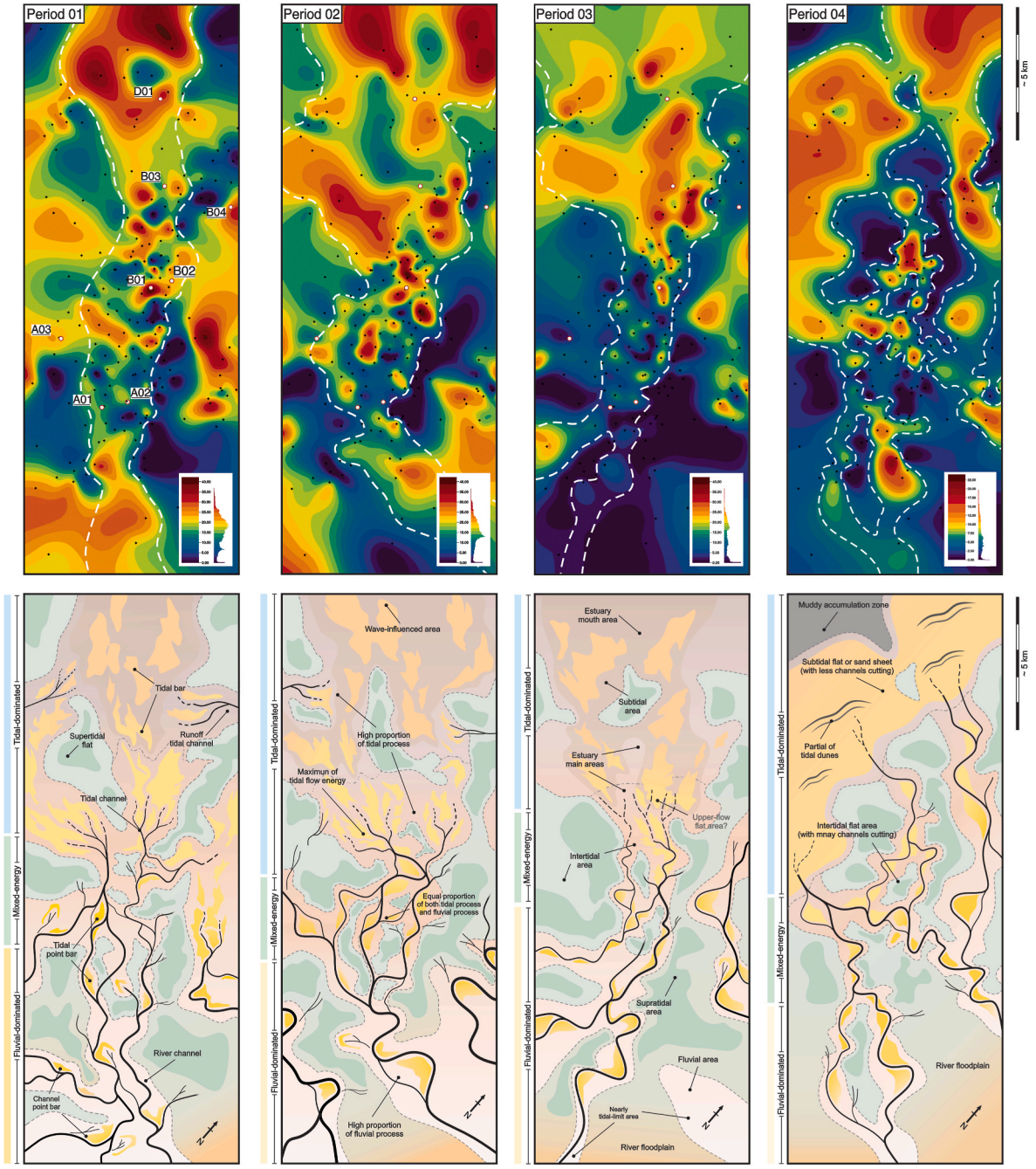

Fig. 16. Isopach map of sand thickness and diagram of probability facies of the four stages in the M1 Sandstone Formation, showing the hydrodynamic processes on the left side of each map. The regional boundary is shown in Fig. 2A. Facies types, hydrodynamic process distributions, and major depositional areas of the estuarine environment are sequentially marked on the facies maps for the first three stages of the estuary. In the last diagram, facies types of open coastal tidal flat are marked. Note that the distribution of sand thickness and facies types on the map is based on the GR logging data and facies interpretation conclusions from 220 wells (including 8 core wells).

5.2.2. Paleogeographic model of the M1 sandstone formation

The interpretation of the depositional environment of the M1 sandstone formation is controversial, despite the general consensus on the presence of a Campanian paleo-shoreline in the eastern slope region of the Oriente Basin (White et al., 1995; Estupiñan et al., 2010; Scotese, 2021). Based on data from the T Block, Ye (2014) interpreted the environment of this region as tide-dominated estuarine deposits inherited from Uppermost Napo Shale deltas and proposed a model in which the M1 Sandstone Formation experienced a relatively complete transgression-regression-transgression cycle. Vallejo et al. (2017) interpreted the sediments in the more eastern ITT Block, suggesting that residual evidence of an early transgressive estuary was preserved in this region, followed by the development of east-to-west delta progradation during the subsequent regression. Lin (2020) compared more extensive drilling data and U-Pb data from across the entire basin and proposed an improved model. In this model, the M1 sandstone underwent multiple episodes of regression during the transgressive phase, better explaining the accumulation of deltaic evidence within the estuarine sediments. These models explain the relationship between the evolution of clastic coastal environment and relative sea-level changes during the Campanian stage.

In our study, the existing evidence reveals a transgression-dominated

estuarine depositional process, which gradually transitions into a highstand open coast tidal flat environment. This transition suggests that the M1 Sandstone Formation may correspond to a complete transgression-regression third-order cycle. This understanding does not contradict previous models. It should be noted that, due to the limited rock record and the redistribution of early deposits by high-energy condition, we did not observe evidence of progradational deltas within the estuarine sediments in this area. However, despite this, we do not rule out the possibility of multiple subordinate regressive episodes, as indicated in Lin's model.

Based on our analysis of sequence-controlling factors, it is not only sea-level fluctuations but also tectonic influences and regional differences in sediment supply that may affect the evolution of depositional environments along the coastline spanning several hundred kilometers. Based on our analysis of sequence-controlling factors, local variations in tectonic influences and sediment supply may affect the evolution of depositional environments along a coastline spanning several hundred kilometers. The synsedimentary faults near the ITT Block (Díaz et al., 2004) may have controlled environmental development in the southeastern part of the basin, and it is possible that stronger sediment supply occurred in the southeast under the influence of compressional processes during the Campanian stage. This could explain the progradational delta deposits found in the southeastern part of the basin (Vallejo et al., 2017), where the delta at the basin margin may exhibit alluvial characteristics (Fig. 17C). As summarized in our discussion on material source, there are significant differences in sediment provenance between the T Block and ITT Block. This result may indicate that the northern and southern parts of the basin had different sediment supply pathways, leading to distinct environmental evidence in the north and south. Considering all this evidence, the relatively weaker sediment supply in the northern basin does not support the progradation of deltas during the transgression, resulting in a predominantly estuarine depositional pattern. In contrast, the stronger tectonic activity in the south, along with the presence of delta deposits, may indicate robust sediment supply, reflected in a depositional model of residual estuarine sediments and progradational deltas (Fig. 17B). We actually did not propose a new model; we simply pointed out that tectonic activity and sediment supply conditions may lead to different sedimentary records within the basin. It is worth noting that if such a transition in depositional models is possible, there may exist a region where sedimentary records are preserved that lie between these two models.

5.3. Tidal-dominated estuary deposition model

The macroscopic spatial distribution of ancient estuarine sediments is relatively distinct, marked by characteristic facies gradient trends (Tessier et al., 2012b; Ahokas et al., 2014; Phillips et al., 2020a,b; Su et al., 2020). In the description and analysis of core profiles, various depositional features emerge, shaped by the interplay of sedimentary processes dominated by differing hydrodynamic conditions. These features include tidal rhythmites indicating strong tidal influences, lithofacies transition interfaces marking rapid hydrodynamic shifts, and lithological stacking sequences depicting gradual changes in water body energy. Previous studies have shown that sedimentary processes in tidal-dominated estuarine environments display pronounced zonation along the estuary's central axis, with the most variable hydrodynamic conditions transitioning regularly from upstream to downstream (Dalrymple et al., 1992, 2011). Within these zones, strong tidal forces and high-energy water conditions provide ample opportunities for sediment redistribution. Hence, the distribution of sediment grain size and depositional structures is somewhat predictable, though the boundaries of facies classification zones in tidal-dominated estuaries remain somewhat indistinct (Phillips et al., 2020a,b). The cyclical variations in facies sequences mirror the mixed hydrodynamic changes within the estuarine environment. Building on the relationship between facies associations, we have devised a facies distribution model for the tidal-dominated estuary (Fig. 18A), which predominantly features upstream fluvial-dominated tidal point bar deposits, mid-section mixed energy interaction zones, and downstream tidal-dominated open-type tidal sand bar deposits. This model also incorporates open-coast tidal flats situated at the top of the estuarine sediments during the late stages of marine transgression. These fine-grained facies successions, with an accurate rhythmic distribution, exhibits lateral zoning characteristics above the estuarine deposits.

5.3.1. Upstream fluvial-dominated zone

As rivers transport sediment into the upstream area of the estuary, these sediments are captured and undergo an initial transport stage influenced by both fluvial and tidal processes. In this region, fluvial dynamics play a dominant role, and the upper estuarine area exhibits sedimentary features akin to a river environment. Governed by one or more main channels, this zone is characterized by sandy sediments primarily consisting of point bars with notable thickness and a gravel component at the base (Fig. 18A). Theoretically, rapid sea level fluctuations dictate cyclical base level changes in the river area, influencing the migration of river channels and the distribution of sediments over a

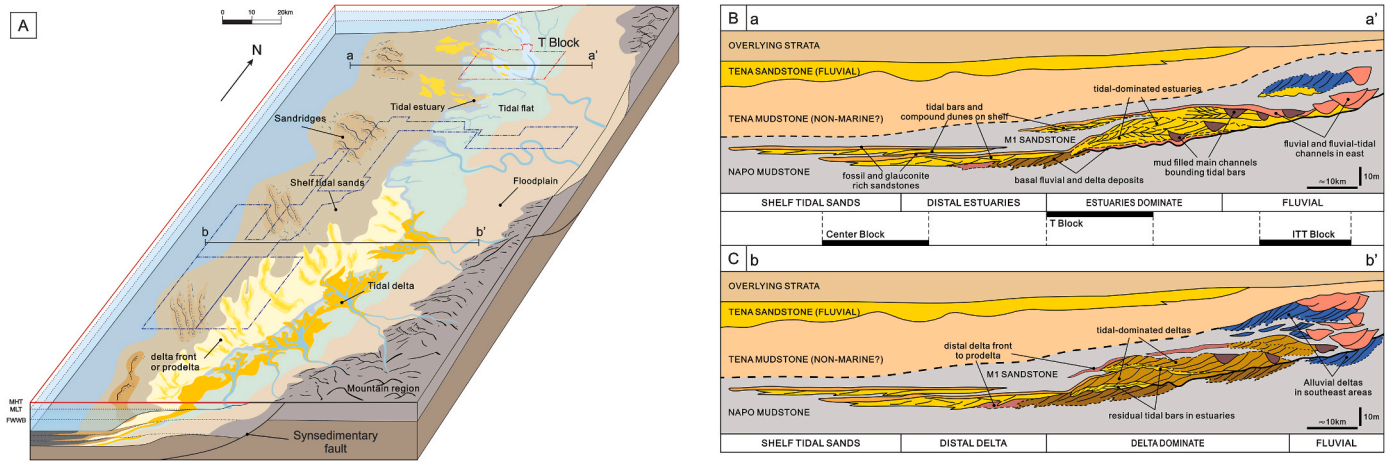

Fig. 17. (A) Environmental distribution trend near the clastic coastline during the Campanian in Oriente Basin. (B) Under the constraint of weak sediment supply in the northern part of the basin, a tide-dominated estuarine depositional model developed. (C) Under the constraint of strong sediment supply in the south part of the basin, a depositional model dominated by residual estuaries and progradational deltas developed (modified from Lin, 2020).

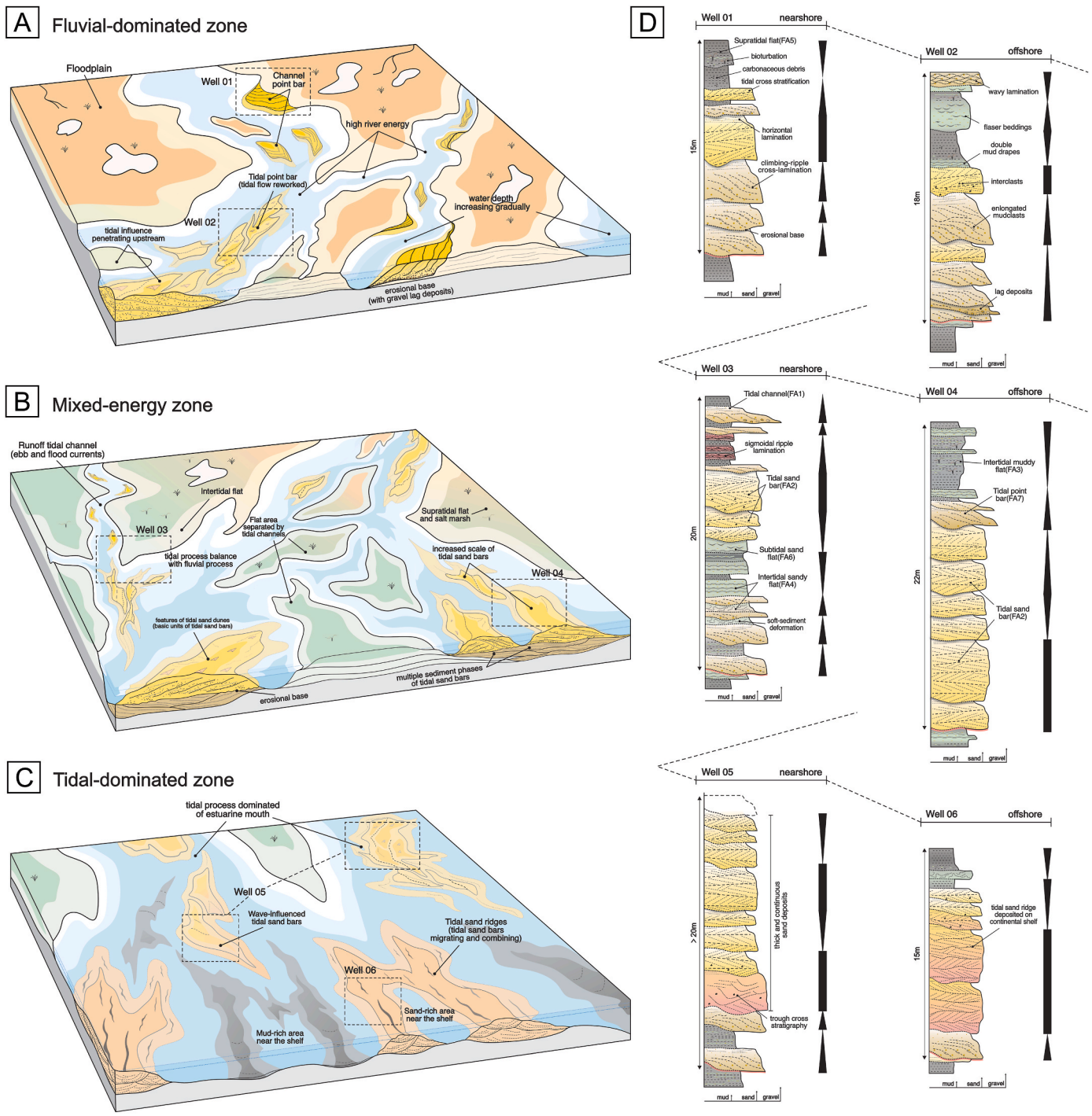

Fig. 18. (A) The sedimentary model of the tidal-dominated estuary, divided into three zones from nearshore to offshore controlled by different hydrodynamic processes, showing the areal distribution of facies and geomorphology. (B) Vertical succession model of the facies sequences, showing the trend of base level changes. Note that the distribution of Well 1 to Well 6 are from nearshore to offshore in sequence.

broader area, including mudflats and salt marsh regions. As variables like river flow and water depth evolve, the river's continual meandering creates a stacked vertical pattern of facies successions characterized by multiple phases of point bar stacking (Fig. 18B). Scour surfaces indicated by flow ripple lamination are frequently observed in the rock record. Furthermore, during marine transgressions, tidal sand bar facies gradually migrate upstream, appearing at the upper part of previous point bar sequences with erosional contact (Fig. 18B).

5.3.2. *Middle mixed-energy interaction zone*

In the energy mixing zone of the estuary, the river gradually converges with tidal currents after crossing the tidal limit (Jablonski and Dalrymple, 2016). Due to the differing net migration directions of the two water bodies, their energies counterbalance when superimposed, forming a relatively stable hydrodynamic mixing zone (Dalrymple et al., 2011; Saha et al., 2018). However, factors such as topographic slope, river flow, and tidal range affect the extent of this mixing zone.

This zone acts as the transitional zone between river-dominated and tidal-dominated regions, serving as the confluence of marine and

terrestrial water bodies. The interplay of tidal and fluvial forces neutralizes the energy of the water bodies, establishing equilibrium at a specific point. In alignment with the facies distribution proposed by Dalrymple et al. (2011), this zone extends upstream to the distal part of the single main river channel and connects downstream with the upper-flow-regime sand flats region. The facies classifications transition in a gradient from river channel facies through distributary tidal channel facies to tidal flat facies (predominantly intertidal) and proximal tidal sand bar facies further downstream (Fig. 18A). The presence of soft-sediment deformation structures and intertidal sand flats indicates that the area still endures strong hydrodynamic conditions. The asymmetry of the tides and the expansion of the topography prompt a single river channel to gradually differentiate into multiple distributary tidal channels, subdividing the tidal flat or proximal sand bar facies into smaller segments. In the succession model of facies associations, tidal channel facies and tidal flat facies are thin and appear alternately, mirroring rapid changes in base level cycles (Fig. 18B). Due to the depth constraints upstream, the development of proximal tidal sand bar facies is also limited. However, as marine transgression progresses and accommodation space expands, tidal sand bars exhibit a trend of stable growth. As these sand bars continue to migrate upstream, they are accompanied by erosion of the underlying sediments.

5.3.3. Downstream tidal-dominated zone

When clastic materials from both land and sea converge at the estuarine mouth, tidal-driven hydrodynamic processes sort these sediments. Coarser sand components are retained and accumulate here, forming tidal sand bars (Virolle et al., 2020). These sand bars are primarily distributed in the intertidal and subtidal zones of the estuarine mouth (Fig. 14A). In estuarine environments with a stable sediment supply, the scale and grain size distribution of tidal sand bars correlate with water depth and flow velocity. Typically, the grain size fines upward. However, actual core observations reveal minimal variation in the grain size, with only a thin layer of fine-grained deposits appearing at the top of each bar facies sequence. This relatively uniform bar accretion sequence (Fig. 18B) indicates a balance maintained between sediment supply and water deepening at the estuary mouth. Under favorable water depth conditions, wave can still influence the bar sediments. As the estuary extends downstream and its width expands, the dominant channels of tidal flow diverge, preventing sandy sediments from fully covering the estuarine area, thus reducing their thickness. At the estuary's farthest reach, it gradually transitions into zones of sandy and muddy aggregation (Fig. 18B), with meters in the outermost part of the estuary showing a homogeneous rhythmic mud or sand throughout the well section (Fig. 8).

5.4. M1 sandstone formation environmental evolution model

Based on the sedimentary dissection results of the M1 Sandstone Formation, a tidal-dominated estuarine sequence evolution model during regressive-transgressive cycles has been established (Fig. 19). This model outlines that the high-energy coastal area where the tidal-dominated estuary developed underwent three primary evolutionary sequences. The first stage represents the initial phase of the evolutionary sequence, corresponding to the early stage of regression-transgression, which is characterized by the development of fluvial systems and incised valleys. The formation of these incised valleys dictates the subsequent evolution sites of the estuary, although sediment evidence is often difficult to preserve. During this period, sea levels were relatively low, keeping the basin margins in a state of low accommodation. River

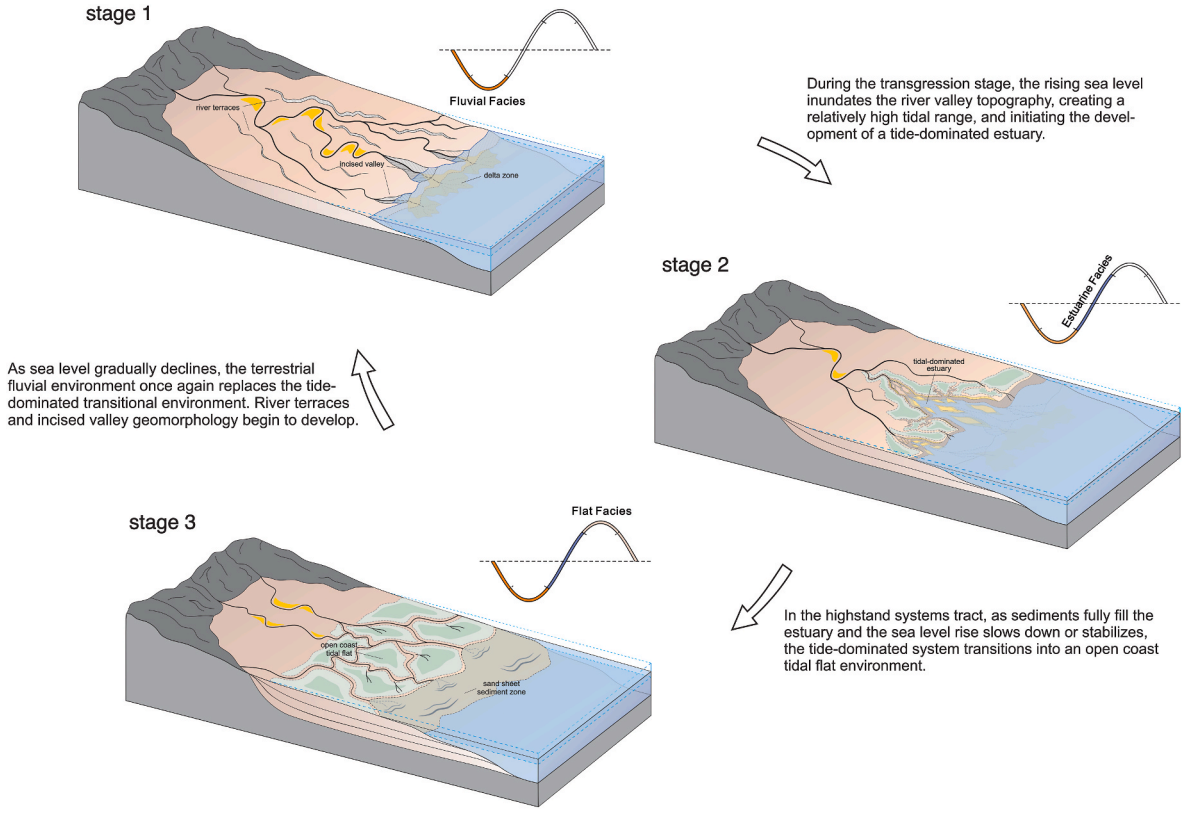

Fig. 19. Conceptual model explaining the evolution of the tidal coastal environments. In Stage 1 (Lowstand systems tract - LST), the emergence of fluvial systems marks the beginning of sequence evolution. Under the erosive action of rivers, incised valleys are formed providing accommodation space for estuary-fill deposits. In Stage 2 (Transgressive systems tract - LST), the inundation of incised valleys by seawater forms estuarine environments. The rapid accumulation of accommodation facilitated the preservation of estuarine sediments in the strata. In Stage3 (Highstand systems tract - HST), separated from the underlying transgressive systems tract by the maximum flooding surface. When sediment supply is slow, tidal flat environments are formed in open coast.

eroded the underlying strata, creating geomorphic depressions, including marginal river terraces and incised valleys. These geomorphic features provided favorable conditions for sediment accumulation and supported a high rate of accommodation growth during the ensuing rapid sea level rise.

The second period marks the sea level rise phase, aligning with the rapid marine transgression stage. During this time, high-energy water bodies dominated by tidal currents flooded the incised valleys, bringing an influx of marine clastic sediments into the estuarine area and enabling rapid development from the early valleys. Sediments were redistributed by mixed hydrodynamic processes dominated by tidal currents, creating sediment convergence zones within the estuary.

The third stage is the highstand systems tract, during which the estuary was filled completely, leading to the development of open-coast tidal flat environments against a backdrop of high energy and gentle shores. With sea-level fluctuations stabilizing, the expansion of accommodation space was constrained, curtailing large-scale erosive actions and the redistribution of sediments (Aschoff and Steel, 2011). During this phase, persistent tidal activities and the shoreline topography facilitated the continuous, slow accumulation of tidal flat sediments near the shoreline, advancing towards the sea. With the onset of the next regression-transgression cycle, river or delta environments began to redevelop. From a sequence evolution standpoint, changes in accommodation space are crucial in driving the evolution of estuarine environments in such coastal areas, where the primary influences are the rate of sediment supply and the long-term modulation of sea-level changes.

6. Conclusions

The Upper Cretaceous M1 sandstone stratum in the Oriente Basin marks the last phase of the marine transgressive cycles of the Napo Formation. This stratum has preserved an extensive collection of tidal-dominated estuarine clastic sediments. It encompasses 14 types of lithofacies and 7 main types of facies associations, which contain many sedimentary structures related to tidal processes. These include bidirectional cross-stratification, tidal rhythmic bedding, double mud drapes, and soft-sediment deformation, each reflecting varying degrees of tidal influence. The diversity of these facies mirrors the evolution of sedimentary processes in stratigraphic spaces, aligning with the varied distribution of facies within sedimentary environments and the estuary developmental phase shifts. The spatial variation trend of the facies associations has subdivided the M1 Sandstone Formation into four depositional periods: the initial development, rapid development, and decline development stages of the estuary, followed by a development stage of the open coast tidal flat environment. Within the estuary's depositional periods, the facies sequences display a consistent alignment trend along the perpendicular direction to the shoreline. The facies associations evolve from discrete tidal point bars to continuous tidal sand bars extending seaward. In the open coast tidal flat environment, this trend transitions to a pattern alternating between tidal flat facies and tidal point bar facies.

In the hydrodynamic analysis, tide plays a significant role, peaking in the sand bar stacked zone near the outer estuary—a predominantly tidal zone. As water depth decreases, the share of tidal processes gradually lessens. Upstream, the growing influence of river dynamics creates zones of mixed energy and river-dominated areas. These hydrodynamic zones correlate with three distinct types of deposit centers, each characterized by unique facies associations. Moreover, in various hydrodynamic zones of the estuary, the absolute energy of the water bodies differs, evident in the well-sorted nature of sediment particle size and thickness scale. Consequently, the relative proportions of different water flows and the absolute energy within the mixed hydrodynamic processes contribute to the deposition and transportation of estuarine sediments to varying degrees.

Finally, we explored a facies model and a sequence evolution model for the development along a broad, gentle shoreline during a persistent marine transgression phase. The Oriente Basin exhibited a low subsidence rate throughout the Late Cretaceous and received a stable sediment supply from the east, fostering ideal conditions for the development of the fluvial-marine transitional environment. The formation of the tide-dominated estuary environment in the M1 sandstone strata was influenced by continuous tectonic subsidence, stable material transport, and predominantly transgressive sea-level changes. The evolution of the tide-dominated estuary initiated in the fluvial incised valley environment during the regressive phase and concluded in the expansive open coast tidal flat environment. The environmental transitions near the ancient shoreline illustrate shifts in accommodation governed by base-level cycles, particularly as the ongoing transgression afforded ample space for the estuary's expansion. By contrast, the facies model of the tide-dominated estuary is shaped by autogenic processes driven by mixed hydrodynamic conditions. The facies of these unique hydrodynamic zones are distinct, serving as indicators for distinguishing the environmental type.

CRediT authorship contribution statement

Sicheng Zhu: Writing – review & editing, Writing – original draft, Visualization, Investigation, Formal analysis, Data curation, Conceptualization. **Panke Sun:** Supervision. **Kexin Zhang:** Resources, Project administration. **Chaoqian Zhang:** Resources, Project administration. **Qi Zhang:** Investigation. **Bin Li:** Visualization. **Jiang Wang:** Visualization. **Shiyi Jiang:** Visualization. **Liyin Bao:** Visualization. **Guangbin Jing:** Visualization. **Zhangxing Chen:** Writing – review & editing, Supervision. **Huaimin Xu:** Validation.

Declaration of generative AI and AI-assisted technologies in the writing process

During the preparation of this work, we used ChatGPT only in order to improve the language and readability. The content of the manuscript has been authored by a human being and the data appearing in the manuscript are real. After using this tool, we have reviewed and edited the content as needed and take full responsibility for the content of the publication.

Declaration of competing interest

The authors declare that they have no known competing financial interests or personal relationships that could have appeared to influence the work reported in this paper.

Data availability

Data will be made available on request.

Acknowledgment

This research is supported by the Research Institute of Petroleum Exploration and Development, PetroChina, and the China Scholarship Council (No.202306440151). We express our gratitude to the staff of the Research Institute of Petroleum Exploration and Development, for their valuable assistance in providing necessary research data. We are grateful to all reviewers for their thorough and constructive reviews, which greatly helped to improve our manuscript. Thanks to Olariu Cornel for the detailed guidance during the manuscript revision phase, especially for the many constructive comments on the discussion section.

References

Aguirre-Urreta, B., Martinez, M., Schmitz, M., Lescano, M., Omarini, J., Tunik, M., Kuhnert, H., Concheyro, A., Rawson, P.F., Ramos, V.A., Reboulet, S., Noclin, N.,

Frederichs, T., Nickl, A.-L., Pälike, H., 2019. Interhemispheric radio-astrochronological calibration of the time scales from the andean and the tethyan areas in the valanginian–hauterivian (early cretaceous). Gondwana Res. 70, 104–132. https://doi.org/10.1016/j.gr.2019.01.006.
Ahokas, J.M., Nystuen, J.P., Martinius, A.W., 2014. Stratigraphic signatures of punctuated rise in relative sea-level in an estuary-dominated heterolithic succession: incised valley fills of the toarcian ostreaelv formation, neill klinter Group (jameson land, east Greenland). Mar. Pet. Geol. 50, 103–129. https://doi.org/10.1016/j.marpetgeo.2013.11.001.
Ainsworth, R.B., Vakarelov, B.K., Nanson, R.A., 2011. Dynamic spatial and temporal prediction of changes in depositional processes on clastic shorelines: toward improved subsurface uncertainty reduction and management. AAPG Bull. 95, 267–297. https://doi.org/10.1306/06301010036.
Aldinucci, M., Ghinassi, M., Sandrelli, F., 2007. Climatic and tectonic signature in the fluvial infill of a late pliocene valley (siena basin, northern apennines, Italy). J. Sediment. Res. 77, 398–414. https://doi.org/10.2110/jsr.2007.039.
Allen, G.P., Salomon, J.C., Bassoullet, P., Du Penhoat, Y., De Grandpré, C., 1980. Effects of tides on mixing and suspended sediment transport in macrotidal estuaries. Sediment. Geol. 26, 69–90. https://doi.org/10.1016/0037-0738(80)90006-8.
Aschoff, J.L., Steel, R.J., 2011. Anatomy and development of a low-accommodation clastic wedge, upper Cretaceous, Cordilleran Foreland Basin, USA. Sediment. Geol. 236, 1–24. https://doi.org/10.1016/j.sedgeo.2010.10.006.
Avellaneda-Jiménez, D.S., Cardona, A., Valencia, V., Barbosa, J.S., Jaramillo, J.S., Monsalve, G., Ramírez-Hoyos, L., 2020. Erosion and regional exhumation of an Early Cretaceous subduction/accretion complex in the Northern Andes. Int. Geol. Rev. 62, 186–209. https://doi.org/10.1080/00206814.2019.1596042.
Baby, P., Rivadeneira, M., Christophoul, F., Barragan, R., 1999. Style and timing of deformation in the Oriente Basin of Ecuador. In: 4th International Symposium of Andean Geodynamics (ISAG99, Gottingen) Extended Abstract, pp. 68–72.
Baby, Patrice, Rivadeneira, Marco, et Roberto Barragán, éd, 2004. La Cuenca Oriente: geología y petróleo. Lima: institut français d'études andines, IRD Éditions, Petroecuador. https://doi.org/10.4000/books.ifea.2971.
Baby, P., Rivadeneira, M., Barragán, R., Christophoul, F., 2013. Thick-skinned tectonics in the Oriente foreland basin of Ecuador. Geol. Soc. Lond. Spec. Publ. 377 (1), 59–76. https://doi.org/10.1144/SP377.
Barragán, R., Baby, P., 2004. Magmatismo alcalino intra-placa en la Cuenca Cretácica Oriente, Ecuador: evidencias geoquímicas, geocronológicas y tectónicas. In: Baby, P., Rivadeneira, M., Barragán, R. (Eds.), La Cuenca Oriente: Geología Y Petróleo. Institut français d'études andines, pp. 69–91. https://doi.org/10.4000/books.ifea.2996.
Barragán, R., Christophoul, F., White, H., Baby, P., Rivadeneira, M., Ramírez, F., Rodas, J., 2004. Estratigrafía secuencial del cretácico de la Cuenca Oriente del Ecuador. In: Baby, P., Rivadeneira, M., Barragán, R. (Eds.), La Cuenca Oriente: Geología Y Petróleo. Institut français d'études andines, pp. 45–68. https://doi.org/10.4000/books.ifea.2992.
Barragàn, R., Àlava, J.T., Jaillard, E., White, H., Montenegro, J., Medina, G., 2005. Lower Maastrichtian syntectonic sedimentation along the Subandean Zone and its relationship with an accretionary event of an oceanic terrane registered in the Cordillera Occidental of Ecuador. In: 6th International Symposium of Andean Geodynamics (ISAG 2005. extended abstracts, Barcelona, pp. 94–97.
Barragán, R., Baby, P., Duncan, R., 2005. Cretaceous alkaline intra-plate magmatism in the Ecuadorian Oriente Basin: geochemical, geochronological and tectonic evidence. Earth Planet Sci. Lett. 236, 670–690. https://doi.org/10.1016/j.epsl.2005.03.016.
Boyd, R., Dalrymple, R., Zaitlin, B.A., 1992. Classification of clastic coastal depositional environments. Sediment. Geol. 80, 139–150. https://doi.org/10.1016/0037-0738(92)90037-R.
Boyd, R., Dalrymple, R.W., Zaitlin, B.A., 2006. Estuary and incised valley facies models. In: Posamentier, H.W., Walker, R.G. (Eds.), Facies Models Revisited, vol. 84. SEPM Spec. Publ, pp. 171–234.
Burchard, H., Schuttelaars, H.M., Ralston, D.K., 2018. Sediment trapping in estuaries. Annu. Rev. Mar. Sci. 10, 371–395. https://doi.org/10.1146/annurev-marine-010816-060535.
Chanson, H., 2011. Tidal bores, aegir, eagre, mascaret, pororoca: theory and observations. WORLD SCIENTIFIC. https://doi.org/10.1142/8035.
Chaumillon, E., Tessier, B., Reynaud, J.-Y., 2010. Stratigraphic records and variability of incised valleys and estuaries along French coasts. Bull. Société Géologique Fr 181, 75–85. https://doi.org/10.2113/gssgfbull.181.2.75.
Chen, Y.-W., Wu, J., Suppe, J., 2019. Southward propagation of nazca subduction along the Andes. Nature 565, 441–447. https://doi.org/10.1038/s41586-018-0860-1.
Collins, D.S., Avdis, A., Wells, M.R., Dean, C.D., Mitchell, A.J., Allison, P.A., Johnson, H. D., Hampson, G.J., Hill, J., Piggott, M.D., 2021. Prediction of shoreline–shelf depositional process regime guided by palaeotidal modelling. Earth Sci. Rev. 223, 103827. https://doi.org/10.1016/j.earscirev.2021.103827.
Coughenour, C.L., Archer, A.W., Lacovara, K.J., 2009a. Tides, tidalites, and secular changes in the Earth–Moon system. Earth Sci. Rev. 97, 59–79. https://doi.org/10.1016/j.earscirev.2009.09.002.
Coughenour, C.L., Archer, A.W., Lacovara, K.J., 2009b. Tides, tidalites, and secular changes in the Earth–Moon system. Earth Sci. Rev. 97, 59–79. https://doi.org/10.1016/j.earscirev.2009.09.002.
Daidu, F., Yuan, W., Min, L., 2013. Classifications, sedimentary features and facies associations of tidal flats. J. Palaeogeogr. 2, 66–80. https://doi.org/10.3724/SP.J.1261.2013.00018.
Dalrymple, R.W., 1992. Tidal depositional systems. In: Facies Models Response to Sea-Level Change, vol. 1992, pp. 195–218.
Dalrymple, R.W., 2021. Sedimentation on high-energy sand flats in the Bay of Fundy: the record of tidal-bore activity and deposition from high-concentration suspensions of sand. Sedimentology 68, 2195–2226. https://doi.org/10.1111/sed.12851.
Dalrymple, R.W., Choi, K., 2007. Morphologic and facies trends through the fluvial–marine transition in tide-dominated depositional systems: a schematic framework for environmental and sequence-stratigraphic interpretation. Earth Sci. Rev. 81, 135–174. https://doi.org/10.1016/j.earscirev.2006.10.002.
Dalrymple, R.W., Makino, Y., Zaitlin, B.A., 1991. Temporal and spatial patterns of rhythmite deposition on mud flats in the macrotidal Cobequid Bay–Salmon River estuary, Bay of Fundy, Canada. In: Smith, D.G., Reinson, G.E., Zaitlin, B.A., Rahmani, R.A. (Eds.), Clastic Tidal Sedimentology, 16. Canadian Society of Petroleum Geologists, Memoir, pp. 127–160.
Dalrymple, R.W., Zaitlin, B.A., Boyd, R., 1992. Estuarine facies models: conceptual basis and stratigraphic implications l. J. Sediment. Res. https://doi.org/10.1306/D4267A69-2B26-11D7-8648000102C1865D.
Dalrymple, R.W., Mackay, D.A., Ichaso, A.A., Choi, K.S., 2011. Processes, morphodynamics, and facies of tide-dominated estuaries. In: Principles of Tidal Sedimentology, pp. 79–107. https://doi.org/10.1007/978-94-007-0123-6_5.
Dalrymple, R.W., Kurcinka, C.E., Jablonski, B.V.J., Ichaso, A.A., Mackay, D.A., 2015. Deciphering the relative importance of fluvial and tidal processes in the fluvial–marine transition. In: Developments in Sedimentology. Elsevier, pp. 3–45. https://doi.org/10.1016/B978-0-444-63529-7.00002-X.
Dashtgard, S.E., La Croix, A.D., 2015. Sedimentological trends across the tidal–fluvial transition, Fraser River, Canada. In: Developments in Sedimentology. Elsevier, pp. 111–126. https://doi.org/10.1016/B978-0-444-63529-7.00005-5.
Dashtgard, S.E., Venditti, J.G., Hill, P.R., Sisulak, C.F., Johnson, S.M., La Croix, A.D., 2012. Sedimentation across the tidal–fluvial transition in the lower fraser river, Canada. Sediment. Rec. 10, 4–9. https://doi.org/10.2110/sedred.2012.4.4.
Desjardins, Patricio R., Buatois, L.A., Mángano, M.G., 2012a. Tidal flats and subtidal sand bodies. In: Developments in Sedimentology. Elsevier, pp. 529–561. https://doi.org/10.1016/B978-0-444-53813-0.00018-6.
Desjardins, P.R., Buatois, L.A., Pratt, B.R., Mangano, M.G., 2012b. Forced regressive tidal flats: response to falling sea level in tide-dominated settings. J. Sediment. Res. 82, 149–162.
Díaz, M., Baby, P., Rivadeneira, M., Christophoul, F., 2004. In: Baby, P., Rivadeneira, M., Barragán, R., Baby, P., Rivadeneira, M., Barragán, R. (Eds.), El pre-aptense en la cuenca oriente ecuatoriana. Institut français d'études andines. https://doi.org/10.4000/books.ifea.2989. La Cuenca Oriente: Geología y petróleo (1-).
Ekwenye, O.C., Nichols, G., Nwajide, S.C., Obi, G.C., Onyemesili, O.C., 2017. An insight into the Eocene tide-dominated estuarine system: implications for palaeoenvironmental and sequence stratigraphic interpretations. Arab. J. Geosci. 10, 371. https://doi.org/10.1007/s12517-017-3150-6.
Estupiñan, J., Marfil, R., Scherer, M., Permanyer, A., 2010. Reservoir sandstones of the cretaceous Napo Formation U and T members in the Oriente Basin, Ecuador: Links between diagenesis and sequence stratigraphy. J. Pet. Geol. 33, 221–245. https://doi.org/10.1111/j.1747-5457.2010.00475.x.
Feldman, H., McCRIMMON, G., Freitas, T., 2008. Fluvial to Estuarine Valley-Fill Models Without Age-Equivalent Sandy Shoreline Deposits, Based on the Clearwater Formation (Cretaceous) at Cold Lake, Alberta, Canada 443–472. https://doi.org/10.2110/pec.08.90.0443.
Fenies, H., Lericolais, G., Posamentier, H.W., 2010. Comparison of wave-and tide-dominated incised valleys: specific processes controlling systems tract architecture and reservoir geometry. Bull. Société Géologique Fr 181, 171–181. https://doi.org/10.2113/gssgfbull.181.2.171.
Fietz, S.W., MacEachern, J.A., Gingras, M.K., Ranger, M., Dashtgard, S.E., 2024. Sedimentological and ichnological variations in fluvio-tidal translating point bars, McMurray Formation, Alberta, Canada. Sedimentology 71, 974–1022. https://doi.org/10.1111/sed.13164.
Ghosh, A., Saha, S., Saraswati, P.K., Banerjee, S., Burley, S., 2009. Intertidal foraminifera in the macro-tidal estuaries of the Gulf of Cambay: implications for interpreting sea-level change in palaeo-estuaries. Mar. Pet. Geol. 26, 1592–1599. https://doi.org/10.1016/j.marpetgeo.2008.08.002.
Gingras, M.K., Zonneveld, J.-P., 2015. Tubular tidalites: a biogenic sedimentary structure indicative of tidally influenced sedimentation. J. Sediment. Res. 85, 845–854. https://doi.org/10.2110/jsr.2015.54.
Gombojav, N., Winkler, W., 2008. Recycling of proterozoic crust in the andean amazon foreland of Ecuador: implications for orogenic development of the northern Andes. Terra. Nova 20, 22–31. https://doi.org/10.1111/j.1365-3121.2007.00782.x.
Gregoire, G., Le Roy, P., Ehrhold, A., Jouet, G., Garlan, T., 2017. Control factors of Holocene sedimentary infilling in a semi-closed tidal estuarine-like system: the bay of Brest (France). Mar. Geol. 385, 84–100. https://doi.org/10.1016/j.margeo.2016.11.005.
Gutiérrez, E.G., Horton, B.K., Vallejo, C., Jackson, L.J., George, S.W.M., 2019. Provenance and geochronological insights into late cretaceous-cenozoic foreland basin development in the subandean zone and Oriente Basin of Ecuador. In: Andean Tectonics. Elsevier, pp. 237–268. https://doi.org/10.1016/B978-0-12-816009-1.00011-3.
Harris, P.T., 1988. Large-scale bedforms as indicators of mutually evasive sand transport and the sequential infilling of wide-mouthed estuaries. Sediment. Geol. 57, 273–298. https://doi.org/10.1016/0037-0738(88)90034-6.
Hayes, M.O., FitzGerald, D.M., 2013. Origin, Evolution, and Classification of Tidal Inlets, pp. 13–33.
Hoekstra, P., Bell, P., van Santen, P., Roode, N., Levoy, F., Whitehouse, R., 2004. Bedform migration and bedload transport on an intertidal shoal. Cont. Shelf Res. 24, 1249–1269. https://doi.org/10.1016/j.csr.2004.03.006.

Hori, K., Saito, Y., Zhao, Q., Wang, P., 2002. Evolution of the coastal depositional systems of the changjiang (yangtze) river in response to late pleistocene-holocene Sea-Level changes. J. Sediment. Res. 72, 884–897. https://doi.org/10.1306/052002720884.

Horton, B.K., 2018. Sedimentary record of Andean mountain building. Earth Sci. Rev. 178, 279–309. https://doi.org/10.1016/j.earscirev.2017.11.025.

Jablonski, B.V.J., Dalrymple, R.W., 2016. Recognition of strong seasonality and climatic cyclicity in an ancient, fluvially dominated, tidally influenced point bar: middle McMurray Formation, Lower Steepbank River, north-eastern Alberta, Canada. Sedimentology 63, 552–585. https://doi.org/10.1111/sed.12228.

Jaillard, E., 2022. Late cretaceous-paleogene orogenic build-up of the Ecuadorian Andes: review and discussion. Earth Sci. Rev. 230, 104033. https://doi.org/10.1016/j.earscirev.2022.104033.

Jaillard, E., Soler, P., 1996. Cretaceous to early Paleogene tectonic evolution of the northern Central Andes (0–18°S) and its relations to geodynamics. Tectonophysics 259, 41–53. https://doi.org/10.1016/0040-1951(95)00107-7.

Jaillard, E., Ordoñez, M., Berrones, G., Bengtson, P., Bonhomme, M., Jime′nez, N., Zambrano, I., 1996. Sedimentary and tectonic evolution of the arc zone of southwestern Ecuador during late cretaceous and early tertiary times. J. South Am. Earth Sci. 9, 131–140.

Jaillard, E., Caron, M., Dhondt, A., Ordoñez, M., Andrade, R., Bengtson, P., Bulot, L., Cappetta, H., Davila, C., Diaz, R., Huacho, J., Huaman, C., Jimenez, D., Jime′nez, N., Montenegro, J., Neraudeau, D., Rivadeneira, M., Toro, J., Villagomez, R., Zambrano, I., 1997. In: Síntesis estratigráfica y sedimentológica del Cretáceo y Paleógeno de la cuenca Oriental del Ecuador. Orstom-Petroproduccion, p. 164.

Jaillard, E., Bengtson, P., Dhondt, A.V., 2005. Late Cretaceous marine transgressions in Ecuador and northern Peru: a refined stratigraphic framework. J. South Am. Earth Sci. 19, 307–323. https://doi.org/10.1016/j.jsames.2005.01.006.

Jay, D.A., Talke, S.A., Hudson, A., Twardowski, M., 2015. Estuarine turbidity maxima revisited. In: Developments in Sedimentology. Elsevier, pp. 49–109. https://doi.org/10.1016/B978-0-444-63529-7.00004-3.

Jo, J., Choi, K., 2016. Morphodynamic and hydrodynamic controls on the stratigraphic architecture of intertidal compound dunes on the open-coast macrotidal flat in the northern gyeonggi bay, west coast of korea. J. Sediment. Res. 86, 1103–1122.

Kostaschuk, R., Best, J., 2005. Response of sand dunes to variations in tidal flow: fraser Estuary, Canada. J. Geophys. Res. Earth Surf. 110. https://doi.org/10.1029/2004jf000176 n/a-n/a.

Li, Shunli, Yu, X., Steel, R., Zhu, X., Li, Shengli, Cao, B., Hou, G., 2018. Change from tide-influenced deltas in a regression-dominated set of sequences to tide-dominated estuaries in a transgression-dominated sequence set, East China Sea Shelf Basin. Sedimentology 65, 2312–2338. https://doi.org/10.1111/sed.12466.

Lin, S., 2020. Provenance, Geochronology and Sedimentary Characteristics of the Campanian M1 Sandstone, Napo Formation, Oriente Basin, Ecuador. University of Texas at Austin, USA (Msc. thesis).

Lin, W., Bhattacharya, J.P., 2020. Depositional facies and the sequence stratigraphic control of a mixed-process influenced clastic wedge in the Cretaceous Western Interior Seaway: the Gallup System, New Mexico, USA. Sedimentology 67, 920–950. https://doi.org/10.1111/sed.12667.

Lin, C.-M., Zhuo, H.-C., Gao, S., 2005. Sedimentary facies and evolution in the Qiantang River incised valley, eastern China. Mar. Geol. 219, 235–259. https://doi.org/10.1016/j.margeo.2005.06.009.

Litherland, M., 1994. The metamorphic belts of Ecuador. Geol. Mag. 134 (6), 877–883. https://doi.org/10.1017/S0016756897297657.

Longhitano, S.G., 2011. The record of tidal cycles in mixed silici–bioclastic deposits: examples from small Plio–Pleistocene peripheral basins of the microtidal Central Mediterranean Sea. Sedimentology 58, 691–719. https://doi.org/10.1111/j.1365-3091.2010.01179.x.

Longhitano, S.G., Mellere, D., Steel, R.J., Ainsworth, R.B., 2012. Tidal depositional systems in the rock record: a review and new insights. Sediment. Geol. 279, 2–22. https://doi.org/10.1016/j.sedgeo.2012.03.024.

Louterbach, M., Roddaz, M., Bailleul, J., Antoine, P.-O., Adnet, S., Kim, J.H., Van Soelen, E., Parra, F., Gérard, J., Calderon, Y., Gagnaison, C., Sinninghe Damsté, J.S., Baby, P., 2014. Evidences for a Paleocene marine incursion in southern Amazonia (Madre de Dios Sub-Andean Zone, Peru). Palaeogeogr. Palaeoclimatol. Palaeoecol. 414, 451–471. https://doi.org/10.1016/j.palaeo.2014.09.027.

Martin-Gombojav, N., Winkler, W., 2008. Recycling of proterozoic crust in the andean amazon foreland of Ecuador: implications for orogenic development of the northern Andes. Terra. Nova 20, 22–31. https://doi.org/10.1111/j.1365-3121.2007.00782.x.

Marzouk, L., Youssef, M., 2008. Relative Sea-Level changes of the lower cretaceous deposits in the chotts area of southern Tunisia. Turk. J. Earth Sci. 17, 835–845.

McDonough, K.J., Cross, T.A., 1991. Late Cretaceous sea level from a paleoshoreline. J. Geophys. Res. Solid Earth 96, 6591–6607. https://doi.org/10.1029/91JB00281.

Melnyk, S., Gingras, M.K., 2020. Using ichnological relationships to interpret heterolithic fabrics in fluvio-tidal settings. Sedimentology 67, 1069–1083. https://doi.org/10.1111/sed.12674.

Nio, S.D., Yang, C.S., 1991. Sea-level fluctuations and the geometric variability of tide-dominated sandbodies. Sediment. Geol. 70, 161–193. https://doi.org/10.1016/0037-0738(91)90140-9.

Peng, Y., Steel, R.J., Rossi, V.M., Olariu, C., 2018. Mixed-energy process interactions read from a compound-clinoform delta (paleo–orinoco delta, trinidad): preservation of river and tide signals by mud-induced wave damping. J. Sediment. Res. 88, 75–90.

Peng, Y., Hagstrom, C.A., Horner, S.C., Hodgson, C.A., Martin, H.K., Leckie, D.A., Pedersen, P.K., Hubbard, S.M., 2022. Low-accommodation foreland basin response to long-term transgression: a record of change from continental-fluvial and marginal-marine to open-marine sequences over 60,000 km2 in the western Canada foreland basin. Mar. Pet. Geol. 139, 105583. https://doi.org/10.1016/j.marpetgeo.2022.105583.

Phillips, S.P., Howell, J.A., Hartley, A.J., Chmielewska, M., 2020a. Tidal estuarine deposits of the transgressive naturita formation (Dakota sandstone): San rafael swell, Utah, U.S.A. J. Sediment. Res. 90, 777–795. https://doi.org/10.2110/jsr.2020.51.

Phillips, S.P., Howell, J.A., Hartley, A.J., Chmielewska, M., 2020b. Tidal estuarine deposits of the transgressive Naturita Formation (Dakota Sandstone): San Rafael Swell, Utah, U.S.A. J. Sediment. Res. 90, 777–795.

Plint, A.G., Wadsworth, J.A., 2003. Sedimentology and palaeogeomorphology of four large valley systems incising delta plains, western Canada Foreland Basin: implications for mid-Cretaceous sea-level changes. Sedimentology 50, 1147–1186. https://doi.org/10.1111/j.1365-3091.2003.00599.x.

Pratt, W.T., Duque, P., Ponce, M., 2005. An autochthonous geological model for the eastern Andes of Ecuador. Tectonophysics 399, 251–278. https://doi.org/10.1016/j.tecto.2004.12.025.

Ray, D.C., Van Buchem, F.S.P., Baines, G., Davies, A., Gréselle, B., Simmons, M.D., Robson, C., 2019. The magnitude and cause of short-term eustatic Cretaceous sea-level change: A synthesis. Earth Sci. Rev. 197, 102901. https://doi.org/10.1016/j.earscirev.2019.102901.

Romeuf, N., Soler, P., Jaillard, E., Aguirre, L., Féraud, G., Ruffet, G., 1995. Middle Jurassic volcanism in the Northern and Central Andes. Rev. Geol. Chile 22 (2), 245–259.

Rossi, V.M., Perillo, M.M., Steel, R.J., Olariu, C., 2017. Quantifying Mixed-Process Variability In Shallow-Marine Depositional Systems: What Are Sedimentary Structures Really Telling Us? J. Sediment. Res. 87, 1060–1074.

Ruiz, G.M.H., Seward, D., Winkler, W., 2007a. Chapter 36 Evolution of the Amazon Basin in Ecuador with Special Reference to Hinterland Tectonics: Data from Zircon Fission-Track and Heavy Mineral Analysis. In: Developments in Sedimentology. Elsevier, pp. 907–934. https://doi.org/10.1016/S0070-4571(07)58036-2.

Ruiz, G.M.H., Seward, D., Winkler, W., 2007b. Chapter 36 Evolution of the Amazon Basin in Ecuador with Special Reference to Hinterland Tectonics: Data from Zircon Fission-Track and Heavy Mineral Analysis. In: Developments in Sedimentology. Elsevier, pp. 907–934. https://doi.org/10.1016/S0070-4571(07)58036-2.

Saha, S., Burley, S.D., Banerjee, S., 2018. Mixing processes in modern estuarine sediments from the Gulf of Khambhat, western India. Mar. Pet. Geol. 91, 599–621. https://doi.org/10.1016/j.marpetgeo.2017.12.010.

Scotese, C.R., 2021. An Atlas of Phanerozoic Paleogeographic Maps: The Seas Come In and the Seas Go Out. Annu. Rev. Earth Planet Sci. 49, 679–728. https://doi.org/10.1146/annurev-earth-081320-064052.

Shanmugam, G., 2000. Tide-dominated estuarine facies in the Hollin and Napo ('T' and 'U') formations (Cretaceous), Sacha Field, Oriente Basin, Ecuador: AAPG Bulletin, v. 84, p. 652-682. 2000. AAPG Bull. 84, 652–682.

Smith, D.G., 1988. Tidal bundles and mud couplets in the mcmurray formation, northeastern alberta, Canada. Bull. Can. Petrol. Geol. 36 (2), 216–219. https://doi-org.ezproxy.lib.ucalgary.ca/10.35767/gscpgbull.36.2.216.

Souza, P., Georgiou, I.Y., Fitzgerald, D.M., Hughes, Z.J., Howes, N.C., Kulp, M.A., 2023. Hydrodynamic controls on sedimentary facies of tidal point bars: A case study in the Georgia coastal plain, USA. Sedimentology 70, 895–926. https://doi.org/10.1111/sed.13060.

Spikings, R., Simpson, G., 2014. Rock uplift and exhumation of continental margins by the collision, accretion, and subduction of buoyant and topographically prominent oceanic crust. Tectonics 33, 635–655. https://doi.org/10.1002/2013TC003425.

Spikings, R., Cochrane, R., Villagomez, D., Van Der Lelij, R., Vallejo, C., Winkler, W., Beate, B., 2015. The geological history of northwestern South America: from Pangaea to the early collision of the Caribbean Large Igneous Province (290–75Ma). Gondwana Res. 27, 95–139. https://doi.org/10.1016/j.gr.2014.06.004.

Spikings, R.A., Cochrane, R., Vallejo, C., Villagomez, D., Van Der Lelij, R., Paul, A., Winkler, W., 2019. Latest Triassic to Early Cretaceous tectonics of the Northern Andes: Geochronology, geochemistry, isotopic tracing, and thermochronology. In: Andean Tectonics. Elsevier, pp. 173–208. https://doi.org/10.1016/B978-0-12-816009-1.00009-5.

Strasser, A., 2018. Chapter Three - Cyclostratigraphy of Shallow-Marine Carbonates – Limitations and Opportunities. In: Montenari, M. (Ed.), Stratigraphy & Timescales, Cyclostratigraphy and Astrochronology. Academic Press, pp. 151–187. https://doi.org/10.1016/bs.sats.2018.07.001.

Stupples, P., Plater, A.J., 2007. Statistical analysis of the temporal and spatial controls on tidal signal preservation in late-Holocene tidal rhythmites, Romney Marsh, Southeast England. Int. J. Earth Sci. 96, 957–976. https://doi.org/10.1007/s00531-006-0134-2.

Su, J., Fan, D., Liu, J.P., Wu, Y., 2020. Anatomy of the transgressive depositional system in a sediment-rich tide-dominated estuary: The paleo-Yangtze estuary, China. Mar. Pet. Geol. 121, 104588. https://doi.org/10.1016/j.marpetgeo.2020.104588.

Sztanó, O., De Boer, P.L., 1995. Basin dimensions and morphology as controls on amplification of tidal motions (the Early Miocene North Hungarian Bay). Sedimentology 42, 665–682. https://doi.org/10.1111/j.1365-3091.1995.tb00399.x.

Tang, M., Lu, S., Zhang, K., Yin, X., Ma, H., Shi, X., Liu, X., Chu, C., 2019. A three dimensional high-resolution reservoir model of Napo Formation in Oriente Basin, Ecuador, integrating sediment dynamic simulation and geostatistics. Mar. Pet. Geol. 110, 240–253. https://doi.org/10.1016/j.marpetgeo.2019.07.022.

Tassinari, C.C.G., Macambira, M.J.B., 1999. Geochronological provinces of the Amazonian Craton. Episodes 22, 174–182. https://doi.org/10.18814/epiiugs/1999/v22i3/004.

Tessier, B., 2012. Stratigraphy of Tide-Dominated Estuaries. In: Davis, R.A., Dalrymple, R.W. (Eds.), Principles of Tidal Sedimentology. Springer, Netherlands, Dordrecht, pp. 109–128. https://doi.org/10.1007/978-94-007-0123-6_6.

Tessier, B., Gigot, P., 1989. A vertical record of different tidal cyclicities: an example from the Miocene Marine Molasse of Digne (Haute Provence, France). Sedimentology 36, 767–776. https://doi.org/10.1111/j.1365-3091.1989.tb01745.x.
Tessier, B., Delsinne, N., Sorrel, P., 2010. Holocene sedimentary infilling of a tide-dominated estuarine mouth. The example of the macrotidal Seine estuary (NW France). Bull. Société Géologique Fr 181, 87–98. https://doi.org/10.2113/gssgfbull.181.2.87.
Tessier, B., Billeaud, I., Sorrel, P., Delsinne, N., Lesueur, P., 2012. Infilling stratigraphy of macrotidal tide-dominated estuaries. Controlling mechanisms: Sea-level fluctuations, bedrock morphology, sediment supply and climate changes (The examples of the Seine estuary and the Mont-Saint-Michel Bay, English Channel, NW France). Sediment. Geol. 279, 62–73. https://doi.org/10.1016/j.sedgeo.2011.02.003.
Tessier, B., Furgerot, L., Mouazé, D., 2017. Sedimentary signatures of tidal bores: a brief synthesis. Geo Mar. Lett. 37, 325–331. https://doi.org/10.1007/s00367-016-0479-x.
Thomas, G., Lavenu, A., Berrones, G., 1995. Subsidence evolution of the northern part of the Ecuadorian Oriente Basin (Upper Cretaceous to Present). C. R. Acad Sci II 320, 617–624.
Todd, B.J., Shaw, J., Li, M.Z., Kostylev, V.E., Wu, Y., 2014. Distribution of subtidal sedimentary bedforms in a macrotidal setting: The Bay of Fundy, Atlantic Canada. Cont. Shelf Res. 83, 64–85. https://doi.org/10.1016/j.csr.2013.11.017.
Vallejo, C., Winkler, W., Spikings, R.A., Luzieux, L., Heller, F., Bussy, F., 2009. Mode and timing of terrane accretion in the forearc of the Andes in Ecuador. In: Backbone of the Americas: Shallow Subduction, Plateau Uplift, and Ridge and Terrane Collision. Geological Society of America. https://doi.org/10.1130/2009.1204(09.
Vallejo, C., Tapia, D., Gaibor, J., Steel, R., Cardenas, M., Winkler, W., Valdez, A., Esteban, J., Figuera, M., Leal, J., Cuenca, D., 2017. Geology of the Campanian M1 sandstone oil reservoir of eastern Ecuador: A delta system sourced from the Amazon Craton. Mar. Pet. Geol. 86, 1207–1223. https://doi.org/10.1016/j.marpetgeo.2017.07.022.
Vallejo, C., Romero, C., Horton, B.K., Spikings, R.A., Gaibor, J., Winkler, W., Esteban, J. J., Thomsen, T.B., Mariño, E., 2021. Jurassic to Early Paleogene sedimentation in the Amazon region of Ecuador: Implications for the paleogeographic evolution of northwestern South America. Glob. Planet. Change 204, 103555. https://doi.org/10.1016/j.gloplacha.2021.103555.
Van Den Berg, J.H., Boersma, J.R., Van Gelder, A., 2007. Diagnostic sedimentary structures of the fluvial-tidal transition zone – Evidence from deposits of the Rhine and Meuse. Neth. J. Geosci. 86, 287–306. https://doi.org/10.1017/S0016774600077866.
Vellekoop, J., Holwerda, F., Prámparo, M.B., Willmott, V., Schouten, S., Cúneo, N.R., Scasso, R.A., Brinkhuis, H., 2017. Climate and sea-level changes across a shallow marine Cretaceous–Palaeogene boundary succession in Patagonia, Argentina. Palaeontology 60, 519–534. https://doi.org/10.1111/pala.12297.
Virolle, M., Féniès, H., Brigaud, B., Bourillot, R., Portier, E., Patrier, P., Beaufort, D., Jalon-Rojas, I., Derriennic, H., Miska, S., 2020. Facies associations, detrital clay grain coats and mineralogical characterization of the Gironde estuary tidal bars: A modern analogue for deeply buried estuarine sandstone reservoirs. Mar. Pet. Geol. 114, 104225. https://doi.org/10.1016/j.marpetgeo.2020.104225.
Visser, M.J., 1980. Neap-spring cycles reflected in Holocene subtidal large-scale bedform deposits: A preliminary note. Geology 8, 543. https://doi.org/10.1130/0091-7613(1980)8<543:NCRIHS>2.0.CO;2.
Wang, Z.B., Jeuken, M.C.J.L., Gerritsen, H., de Vriend, H.J., Kornman, B.A., 2002. Morphology and asymmetry of the vertical tide in the Westerschelde estuary. Cont. Shelf Res. 22, 2599–2609. https://doi.org/10.1016/S0278-4343(02)00134-6.
Wang, R., Colombera, L., Mountney, N.P., 2019. Geological controls on the geometry of incised-valley fills: Insights from a global dataset of late-Quaternary examples. Sedimentology 66, 2134–2168. https://doi.org/10.1111/sed.12596.
Webb, N.D., Seyler, B., Grube, J.P., 2015. Geologic reservoir characterization of Carboniferous fluvio-tidal deposits of the Illinois Basin, USA. In: Developments in Sedimentology. Elsevier, pp. 395–443. https://doi.org/10.1016/B978-0-444-63529-7.00013-4.
Wehrmann, A., 2014. Tidal Depositional Systems. In: Harff, J., Meschede, M., Petersen, S., Thiede, J. (Eds.), Encyclopedia of Marine Geosciences. Springer, Netherlands, Dordrecht, pp. 1–13. https://doi.org/10.1007/978-94-007-6644-0_148-1.
Wells, M.R., Allison, P.A., Piggott, M.D., Gorman, G.J., Hampson, G.J., Pain, C.C., Fang, F., 2007. Numerical Modeling of Tides in the Late Pennsylvanian Midcontinent Seaway of North America with Implications for Hydrography and Sedimentation. J. Sediment. Res. 77, 843–865. https://doi.org/10.2110/jsr.2007.075.
White, H., Skopec, R.A., Ramirez, F., Rodas, J.A., Bonilla, G., 1995. Reservoir characterization of the Hollin and Napo formations, western oriente basin, Ecuador. In: Tankard, A.J., Suarez, S.R., Welsink, H.J. (Eds.), Petroleum Basins of South America: American Association of Petroleum Geologist Memoir, vol. 62, pp. 573–596.
Woodroffe, C.D., Chappell, J., Thom, B.G., Wallensky, E., 1989. Depositional model of a macrotidal estuary and floodplain, South Alligator River, Northern Australia. Sedimentology 36, 737–756. https://doi.org/10.1111/j.1365-3091.1989.tb01743.x.
Yan, D., Xu, H., Xu, Z., Lei, Z., Tian, M., Cheng, L., Ma, Y., Wang, Z., Ostadhassan, M., 2020. Sedimentary architecture of hyperpycnal flow deposits: Cretaceous Sangyuan outcrop, from the Luanping Basin, North East China. Mar. Petrol. Geol. 121, 104593. https://doi.org/10.1016/j.marpetgeo.2020.104593.
Yan, D., Zhu, R., Liu, W., Liu, R., Shou, H., Cheng, X., Cai, Y., Lei, Z., Deng, P., Peng, Y., 2024a. Metallogenic characteristics and models of sandstone-type uranium deposits in China. Ore Geol. Rev. 166, 105937. https://doi.org/10.1016/j.oregeorev.2024.105937.
Yan, D., Zhu, R., Shou, H., Xu, Z., Liu, W., Zhu, S., Lei, Z., Zhang, J., Liu, C., Cai, Y., Xu, H., 2024b. Depositional process of hyperpycnal flow deposits: A case study on Lower Cretaceous Sangyuan outcrop in the Luanping Basin, Northeast China. China Geology 7 (3), 505–516. https://doi.org/10.31035/cg2023096.
Yang, B.C., Dalrymple, R.W., Chun, S.S., 2005. Sedimentation on a wave-dominated, open-coast tidal flat, south-western Korea: summer tidal flat - winter shoreface: Sedimentation on open-coast tidal flats. Sedimentology 52, 235–252. https://doi.org/10.1111/j.1365-3091.2004.00692.x.
Yang, X.-F., Xie, Y.-F., Zhang, Z.-W., Ma, Z.-Z., Zhou, Y.-B., Liu, Y.-M., Wang, D.-D., Zhao, Y.-B., 2017. Hydrocarbon Generation Potential and Depositional Environment of Shales in the Cretaceous Napo Formation, Eastern Oriente Basin, Ecuador. J. Pet. Geol. 40, 173–193. https://doi.org/10.1111/jpg.12671.
Ye, Y., 2014. Depositional Systems and Sequence Stratigraphy of the M1 Sandstone in Tarapoa, Ecuador (Msc. Thesis). University of Texas at Austin, USA.
Yoshida, S., Jackson, M.D., Johnson, H.D., Muggeridge, A.H., Martinius, A.W., 2001. Outcrop Studies of Tidal Sandstones for Reservoir Characterization (Lower Cretaceous Vectis Formation, Isle of Wight, Southern England). Norwegian Petroleum Society Special Publications. Elsevier, pp. 233–257. https://doi.org/10.1016/S0928-8937(01)80016-3.
Yoshida, S., Steel, R.J., Dalrymple, R.W., 2007. Changes in Depositional Processes–An Ingredient in a New Generation of Sequence-Stratigraphic Models. J. Sediment. Res. 77, 447–460. https://doi.org/10.2110/jsr.2007.048.
Zamora, G., Gil, W., 2018. The Marañón Basin: Tectonic Evolution and Paleogeography. In: Petroleum Basins and Hydrocarbon Potential of the Andes of Peru and Bolivia. The American Association of Petroleum Geologists, pp. 121–144. https://doi.org/10.1306/13622119M1173768.
Zhang, X., Lin, C.-M., Dalrymple, R.W., Gao, S., Li, Y.-L., 2014a. Facies architecture and depositional model of a macrotidal incised-valley succession (Qiantang River estuary, eastern China), and differences from other macrotidal systems. Geol. Soc. Am. Bull. 126 (1), 499–522. https://doi.org/10.1130/B30835.
Zhang, X., Lin, C.-M., Dalrymple, R.W., Gao, S., Li, Y.-L., 2014b. Facies architecture and depositional model of a macrotidal incised-valley succession (Qiantang River estuary, eastern China), and differences from other macrotidal systems. Geol. Soc. Am. Bull. 126 (1), 499–522. https://doi.org/10.1130/B30835.
Zhongzhen, M., Heping, C., Xiaofa, Y., Yubing, Z., Zuoji, T., Dandan, W., Yaming, L., Yongbin, Z., 2021a. Geochemical Characteristics and Charge History of Oil in the Upper Cretaceous M1 Sandstones (napo Formation) in Block T, Oriente Basin, Ecuador. J. Pet. Geol. 44, 167–186. https://doi.org/10.1111/jpg.12784.
Zhongzhen, M., Heping, C., Xiaofa, Y., Yubing, Z., Zuoji, T., Dandan, W., Yaming, L., Yongbin, Z., 2021b. Geochemical Characteristics and Charge History of Oil in the Upper Cretaceous M1 Sandstones (napo Formation) in Block T, Oriente Basin, Ecuador. J. Pet. Geol. 44, 167–186. https://doi.org/10.1111/jpg.12784.
Zhou, Z., Liu, Q., Fan, D., Coco, G., Gong, Z., Möller, I., Xu, F., Townend, I., Zhang, C., 2021. Simulating the role of tides and sediment characteristics on tidal flat sorting and bedding dynamics. Earth Surf. Process. Landf. 46, 2163–2176. https://doi.org/10.1002/esp.5166.
Zhu, S., Sun, P., Zhang, K., Zhang, C., Xu, Z., Xu, H., 2024. Study on a Prediction Method of Hydraulic Units Using Logging Curves Constrained by Complex Lithofacies: A Case Study of the Tidal Estuarine Reservoir in Napo Formation, Oriente Basin. In: Lin, J. (Ed.), Proceedings of the International Field Exploration and Development Conference 2023. Springer Nature, Singapore, pp. 684–699. https://doi.org/10.1007/978-981-97-0468-2_52.
Zuniga, M., Buatois, L.A., Vallejo, C., Mángano, M.G., 2021a. Paleoenvironmental significance of trace fossils from mixed tide- and river-influenced marginal-marine settings, Cretaceous U and M2 Sandstone members, Napo Formation, Oriente Basin of Ecuador. J. South Am. Earth Sci. 110, 103326. https://doi.org/10.1016/j.jsames.2021.103326.
Zuniga, M., Buatois, L.A., Vallejo, C., Mángano, M.G., 2021b. Paleoenvironmental significance of trace fossils from mixed tide- and river-influenced marginal-marine settings, Cretaceous U and M2 Sandstone members, Napo Formation, Oriente Basin of Ecuador. J. South Am. Earth Sci. 110, 103326. https://doi.org/10.1016/j.jsames.2021.103326.